

Detailed computer modeling of semiconductor devices

N Palit, U Dutta and P Chatterjee*

Energy Research Unit, Indian Association for the Cultivation of Science, Jadavpur, Kolkata-700 032, India

E-mail : parsathi_chatterjee@yahoo.co.in

Received 8 September 2005, accepted 23 November 2005

Abstract : Detailed computer modeling to optimize the performance and design of semiconductor devices in general and of solar cells in particular has become extremely popular over the last two decades. This is because, experimentally, such optimization involves a huge number of trials; whereas the number of trials needed to optimize the performance of such semiconductor devices, can be decimated, using computer modeling, which is nowadays therefore widely recognized as a tool for faster progress of such research. A detailed computer model, as opposed to simple analytical models, is where the Poisson's equation and the electron- and hole-continuity equations are all solved from the first principles, without resorting to any simplifying assumptions. It is therefore, only such detailed models that are capable of giving an insight into device performance. Such models become very complicated in the case of disordered semiconductors, where we also have to take into account the trapping and recombination kinetics through the gap states. Moreover, in order to model both the electrical and optical properties of opto-electronic devices based on semiconductors in their entirety, we also need to combine the electrical model with a suitable optical model, capable of calculating not only the absorption in each portion of the device, but also the losses suffered by reflection or absorption in the non-active layers of the device. Moreover, diffused reflectance, transmittance and absorption when the device is deposited on a textured or rough surface also need to be taken into account; as also specular interference effects when the interfaces are flat. In this review, we will discuss a detailed electrical-optical model that is capable of modeling the performance of a general n -layer device based on crystalline, amorphous, poly-, micro- or nano-crystalline semiconductor, with particular reference to the modeling of opto-electronic devices, such as solar cells and color sensors.

Keywords : Detailed computer modeling, amorphous and disordered semiconductors, solar cells, electrical model, optical model, gap-state model.

PACS Nos. : 85.30.De, 84.60.Jt

Plan of the Article

1. Introduction

2. Review of electrical model

3. Review of optical model and integrated electrical-optical model

4. Dynamic inner collection efficiency in a-Si:H based PIN solar cells

5. Description of a typical detailed one-dimensional electrical-optical model (ASDMP)

5.1. Electrical model

5.1.1. Calculation of the net charge density

5.1.2. Recombination through localized states

5.1.3. Expressions for J_n , J_p

5.2. Calculation of dark reverse bias current taking into account high field emission under reverse bias conditions

5.3. Calculation of the position-dependent inner carrier collection efficiency (PDICE) in solar cells

5.4. Generation/optical model

5.5. Solution technique

5.5.1. Thermodynamic equilibrium

5.5.2. Non-thermodynamic equilibrium steady state

6. Typical results for a single junction a-Si:H based solar cell : calculations based on ASDMP

7. Summary

8. Future outlook

*Corresponding Author

1. Introduction

In the past two decades, computer modeling of solar cell structures has become an increasingly popular tool for analyzing the performance of solar cells and for optimizing the design of crystalline, polycrystalline and amorphous semiconductor devices. There is no doubt that the role of device modeling will increase further in future. But, setting up these models is not easy, especially where the semiconductor material is a disordered one, with many defect states in the forbidden energy gap. Detailed computer modeling is very complicated, requiring knowledge of a large number of input parameters. Moreover, the results produced by such a model are obtained in a tabular form, or in the form of graphs, which makes it quite difficult to grasp the controlling physics. Simple analytical models on the other hand, do not require all the parameters and the results can be captured in simple analytical expressions. In spite of the above-mentioned difficulties in detailed computer modeling, the emphasis on the latter is due to the fact that we aim to get solar cells of the highest efficiency. To achieve this, it becomes essential to gain a full understanding of the device physics and explore fully the solar cell structures. When we are trying to understand every detail of solar cell performance and squeeze out every bit of efficiency possible, all the parameters that detailed computer-modeling need as input must be considered. In the analytical models simplifying assumptions to the transport equations are used to avoid numerical integration of the Poisson's and continuity equations. Such analytical models, therefore, are only as good as these approximations and in order to get a full insight into device performance, there is no alternative to detailed computer modeling. Our definition of the latter is the approach where Poisson's equation and the continuity equations are all solved rigorously without any simplifying assumptions, using numerical techniques.

Detailed computer models deliver as output : (i) external properties of a device that are measurable quantities, (ii) internal properties of a device that cannot be measured directly, or cannot be measured at all. In the case of solar cells, the dark and the illuminated current density-voltage (J - V) characteristics and the quantum efficiency (QE) are the external properties. The electric field, the concentration of free and trapped charge carriers, the space charge, the electron and hole current densities and the recombination rate as a function of the position in the solar cell, are its internal properties. An

important step in modeling is accurate calibration of model parameters, *i.e.* assignment of proper values to the input parameters. The calibration procedure is based on comparison of the simulated external properties with experimental data. If the calibrated computer model reproduces a broad range of experimental results, then only can one be confident about the correctness of the model and the fact that the values used for the input parameters correctly represent the device being modeled. One can then use these parameters to optimize the solar cell or detector structure, *etc.*, as the case may be, for the best performance. This procedure of model development, model calibration, prediction, and derivation of the model from experiments, contribute to a better knowledge of the material properties and the physics controlling the device operation.

Most of the simulation programs were initially designed for crystalline semiconductor devices [1,2]. These programs were based on the solution of semiconductor equations, and on the physical models that describe the semiconductor material properties. This approach can also be used in modeling a-Si:H based devices. However, in the case of a-Si:H, special attention has to be paid to model the continuous distribution of localized states in the band gap and the recombination-generation (R-G) statistics of these states.

Since, Swartz [3] introduced detailed *ab initio* numerical device modeling in 1982 to study hydrogenated amorphous silicon solar cells, device simulators are being used in the a-Si:H photovoltaic research community. In the course of time, various simulation programs have been developed especially for a-Si:H solar cells. Different independent variables (quasi-Fermi levels, carrier population) are chosen in the different models. Different programs use different solution techniques. One of the most important intrinsic properties of a-Si:H is the density of localized states in the gap. Charge carriers in these states do not take part in drift and diffusion currents, but they significantly influence recombination of light-generated carriers and also affect the space-charge distribution, which, in turn, modifies the magnitude and distribution of the built-in electric field inside the multi-layered a-Si:H solar cell structure. To describe these localized gap states, different density of states (DOS) models have been used in the different programs. Contact treatments also differ in different models.

In order to simulate the performance of the present day state-of-the-art solar cell in its entirety, both the

electrical and the optical properties have to be investigated. Thus, two aspects of computer modeling of a-Si:H based solar cells have become important : one deals with the electrical transport of the charges, their recombination, trapping, mobility *etc.*, while the other aspect deals with the optical generation of electron-hole pairs, their absorption, reflection and transmission in the different layers. In the following, a historical background of both the electrical and optical models is discussed separately in brief.

2. Electrical model

As already stated, in detailed *ab initio* computer modeling, the Poisson's equation and the two carrier continuity equations are simultaneously solved using rigorous numerical techniques under non-thermodynamic equilibrium steady-state conditions (*i.e.* under light or voltage bias or both). Swartz [3] of RCA laboratories developed the first comprehensive computer model of an amorphous silicon *PIN* solar cell in 1982. In this work, he used Scharfetter- Gummel trial functions [4]. He, however, assumed for simplicity a single level Shockley-Read-Hall (SRH) recombination model [5,6] (a-Si:H has a complicated DOS with a number of levels inside the band gap participating in the recombination process) and ignored trapped charges in the intrinsic(*I*)-layer. The latter assumption is also incorrect because trapped charge dominates the space charge in amorphous semiconductor materials. Also the model did not address transport or electrostatics in the doped regions; instead assuming boundary conditions at the *P/I* and *N/I* interfaces.

At about the same time, Chen and Lee [7] also developed a model that used a numerical solution scheme based on the integral technique to solve the Poisson's equation and the continuity equations. Here, the equations were solved using an iterative relaxation technique. Like Swartz's model, this model also assumed a single level SRH model to compute recombination. Hence this model also did not account for recombination properly. However, they introduced band tails in their DOS picture. These tails were only allowed to trap charges; however recombination through these states was not considered. But they did use Fermi statistics to calculate the space charge density in the tail states. In their model, the electron and hole concentration at the front and back contacts were fixed at their thermodynamic equilibrium values, which means that they considered ideal ohmic contacts.

In the next two years, a sort of combined analytical-numerical approach was used by some investigators. This type of approach uses various approximations to the transport equations to permit closed-form solutions and to avoid numerical integration of the continuity and Poisson's equations. However, numerical techniques were then often used in solving the resulting algebraic equations. Crandall [8], Okamoto *et al* [9], Sichenugrist *et al* [10,11] and Faughnan *et al* [12,13] have used this approach to solve the transport equations. Some of the simplifying assumptions used by this group are constant minority carrier lifetimes in amorphous semiconductors, invariant drift mobilities and they implied that the field profile and charge distribution were entirely controlled by the intrinsic layer. Crandall [8] also assumed a constant electric field over the *i*-layer. The doped regions as well as the contact to these regions were not considered properly. Thus, for the above reasons, analytical models are only as good as their assumptions. They may be utilized to give a patch up explanation to experiments. But they cannot introduce any new concept to improve the efficiency or help refine our understanding of the physics of solar cells.

From 1985, we find a spurt of activities in the *ab initio* detailed modeling sector. Ikegaki *et al* [14] developed a computer model similar to reference [7]. It too allowed for a single recombination level. However, rather than assuming ohmic contacts, they used recombination velocities at the *P/I* and *N/I* interfaces as boundary conditions. Thus, they too did not consider the transport kinetics in the doped layers.

It was Hack and Shur [15] who published the first detailed computer model of solar cells that allowed a more complete DOS picture in the band gap, and for the first time, took into account both recombination and charge storage (trapping) in these states. The model used two exponential acceptor-like tails emerging from the conduction band and two exponential donor-like tails emerging from the valence band. The occupancy in these states were also calculated using the Taylor-Simmons' approximation ($T = 0^\circ\text{K}$ occupation function) [16]. In addition, the Hack and Shur model [15] took into account the transport kinetics in the doped layers; although the boundary conditions used were still ideal ohmic contacts. At about the same time, Schwartz [17] developed a similar model independently that allowed for an even more general DOS picture. In its more developed form this model introduced amphoteric dangling bond states in the gap where occupancy was determined by the statistics

developed by Sah [18]. The model initially assumed ideal ohmic contacts only but this restriction was removed with subsequent work. Pawlikiewicz *et al* [19] developed a model on the lines of Hack and Shur [15] with a two donor-two acceptor tail states. However, the band related properties were allowed to vary with position. But, these authors assumed ideal ohmic contacts at the boundary. Tasaki *et al* [20] developed a model which tried to address the physics in a-Si:H based *PIN* hetero junction solar cells for the first time. Besides tail states, it considered the distribution of deep dangling bond states *via* two delta functions. However, the contacts were still considered to be ideally ohmic and the Taylor-Simmons' (0°K) approximation [16] was used to compute trapped charge and recombination through the localized gap states.

Another significant model to explain the performance of a-Si:H based solar cells was developed by Misiakos and Lindholm [21] at the same time. Like that of Hack and Shur, this model used exponential distribution for acceptor and donor states in the bandgap. Taylor-Simmons' approximation was also used here to compute the recombination and the trapped charges in the defect states. The boundary conditions for the minority carriers were surface recombination speeds that characterize minority carrier flow across the contacts. However, the majority carrier concentrations were assumed to be the same in thermodynamic equilibrium and under different voltage bias and illumination conditions.

The computer model AMPS developed by Fonash *et al* [22–24] requires to be mentioned next. It was revised later by Hou *et al* [25] and Rubinelli *et al* [26]. Trapping and recombination in the AMPS model was determined using the Shockley-Read-Hall formalism, taking proper account of the ambient temperature. In other words, the Taylor-Simmons' (0°K) approximation was not employed. AMPS takes into account the effective force-fields caused by drift, diffusion, bandgap and affinity variations. The material properties were allowed to vary with position and the gap state properties with both position and energy. The boundary conditions were also general, requiring the electrostatic energy of the vacuum level (for the Poisson's equation) and the hole and electron recombination speeds of the transparent conducting oxide (TCO)/*P* and *N*/metal contacts (for the two continuity equations) to be specified. It takes into account both charge storage and recombination through the band tail states and the dangling bond states. In the final form [26], the latter is modeled by Gaussian

distribution functions. This model also allows for direct hole tunneling at the front contact [27]. The same group in 1991 first formulated the strategy to simulate the contact region between two subcells of a multi-junction structure. The junction was modelled by a thin, highly defective, recombination layer with a reduced mobility gap. The potential barriers for carriers moving towards this region were reduced by band gap grading.

Mittiga *et al* [28] developed a simplified model which qualitatively explains the complete simulation results to study the dark *J-V* characteristics of *PIN* a-Si:H solar cells. They used the Gaussian distribution model of one electron states for the gap states. This gap state distribution could not completely account for correlation effects but was found to be a good approximation always in computing the recombination and trapped charges. They however chose equal carrier band microscopic mobilities for electrons and holes, which is unphysical. Ohmic contacts were used by them at the boundaries. Also, at the same time, another device model for amorphous silicon based tandem solar cells was developed for direct simulation of the characteristics of the tandem structure [29]. The model was implemented in the developed one-dimensional device simulator called AMO1 where the Shockley-Read-Hall statistics was used to calculate the electron occupancy of the states. Both ohmic contacts at the electrode-semiconductor interface and Schottky barrier contact boundary conditions at the *N-P* junction between *PIN* sub-cells in a multi-junction structure were used. Tandem cells have been modeled by two *PIN* cells in series and thus proper consideration of the physics of carrier transport at the junction of the two sub-cells has not been taken into account in this model. The potential at the tandem interface between the cells is consistently set at the position of the half the applied voltage to maintain the current continuity.

In 1992, another model was developed by Chatterjee of the Indian Association for the Cultivation of Science, Kolkata, India, that is similar to the AMPS model [30]. This program also introduced a donor-like and an acceptor-like Gaussian distribution function to simulate trapping and recombination through the deep dangling bond states, independently in 1992. The exponential band-tails were also, of course, present. Recombination and charge trapping in the defect states were considered using the Shockley-Read-Hall statistics. This electrical model has been used to simulate the *J-V* and *Q-E* characteristics of single [31, 32] and double junction [33]

cells. It has also been applied to study the properties of a-Si:H based temperature sensors [34] and investigate the origin of current gain in amorphous silicon *N-I-P-I-N* structures (colour sensors) [35]. This program, which is very similar to the AMPS program, has been used for all calculations in this study. It will be described in detail later. Smole *et al* [36] developed the ASPIN model. Shockley-Read statistics [5,6] was used to calculate the recombination and charge trapping. In addition to tails of donor-like and acceptor-like states, three Fermi-energy dependent defect states densities D^- , D^0 , D^+ , described by Gaussian distribution functions, with their correlated states according to the defect pool model were also used. Smole *et al* [37] also included in their device modeling program, the transparent conducting oxide (TCO) layer.

In the meantime, another model (ASA) was developed by Zeman *et al* [38-41]. This model has the advantage of simulating quasi steady-state capacitance-voltage (*C-V*) characteristics, in addition to the steady-state characteristics. There is provision here to either use the ‘standard’ model (exponential tail states and deep dangling bond states simulated by a donor-like and acceptor-like Gaussian distribution function) or the defect pool model, where a amphoteric three-states model is used to calculate recombination and charge trapping. ASA is also equipped with the trap-assisted tunneling recombination model of Hurkx *et al* [42], which models the field-dependent recombination in high-field regions of the device such as the junction region between two subcells of a multi-junction structure. This trap assisted tunneling model yields a much higher recombination in the space charge regions by taking into account an increased carrier concentration at a recombination centre, resulting from tunneling from nearby locations and gives a modification of the well known Shockley-Read-Hall formula for recombination. But, the application of the trap assisted tunneling model alone was not sufficient to simulate the *J-V* characteristics of the tandem cells due to the fact that the tunneling model does not account for the tunneling transport towards the recombination sites. It was found by Willemen *et al* [41] that this could be accomplished by increasing the extended state mobility in high field regions and they have used a constant increased mobility in high field regions. Based on experimental evidence, that room-temperature drift mobility increases exponentially in fields above 10^5 V/cm [43,44], they applied the following formula to the usual extended state mobilities μ_{ext} .

$$\mu_{\text{eff}} = \mu_{\text{ext}} \cdot \exp\left(\frac{|E|}{E_0}\right) \quad (1)$$

where the electric fields $|E|$ are the thermal equilibrium values and μ_{eff} stands for the effective mobility. With the parameter value $E_0 \approx 2 \times 10^5$ V/cm, they obtained good results.

The model ASCA was developed by Martins *et al* [45]. This model is able to describe both the transient and steady-state behavior of solar cell devices. It can be used to simulate the time-degradation dependence ascribed to changes in DOS. The ‘standard’ gap state model was used. However, the majority carrier density at the front and back contacts was chosen to be equal to its value in the thermal equilibrium. A numerical modeling programme was also developed by Kreisel [46] to study the degradation in amorphous silicon based thin film solar cells.

3. Review of optical model and integrated electrical-optical model

In most of the above models, the optical generation term G , in the continuity equations was calculated using a formula based on the simple exponential law of absorption.

Here, $G = \sum_{\lambda} \alpha_{\lambda} \phi_{\lambda} e^{(-\alpha_{\lambda} x)}$ and represents the photo-generation due to light of an arbitrary spectrum where

the incident flux of each component wavelength λ , characterized by an absorption coefficient of α_{λ} in the material, is ϕ_{λ} . Constant values were chosen for the reflections at the front and the back surfaces. This simple formula is not able to calculate correctly the absorption inside the device because several aspects have been neglected. The wavelength dependent reflection at the front transparent conducting oxide (TCO), and from the back contact metal and absorption in these two end layers, need to be properly considered. Also light trapping effects due to textured TCO surfaces and specular interference effects when the TCO is flat, should be taken into consideration. A good optical design is one of the key attributes for achieving high-efficiency silicon solar cells. Thus it is important to design a structure in which the absorption of incident light in the active parts of the cell is a maximum. In case of a-Si:H solar cells, several light trapping techniques have been implemented to achieve this aim. These include the introduction of textured (rough) surfaces and the use of special reflector layers to keep light inside the active part of the cell.

With the implementation of various light trapping techniques the cells become very complicated systems and, it becomes essential to replace the above simple and straightforward exponential absorption law by sophisticated optical models. In this approach the solar cell is regarded as a multi-layer thin-film optical system and the optical behavior of this system, which has to take into account reflection and transmission at all interfaces and absorption in all layers of the system, is solved using numerical techniques. The general treatment of optical properties of thin films can be found in several references, *e.g.* Heavens [47]. This treatment uses the complex refractive indices of the media and the effective Fresnel's coefficients. The texture causes scattering of incident light at the interface and in general, the amount and the angular distribution of scattered light depend on the refractive indices of the media, the texture of the interface, and the incident angle. If the exact morphology of the rough interfaces is known, one can apply several approaches such as geometrical optics, physical optics or electromagnetic theory to study the scattering of light at these interfaces. As the texture introduces spatial variations in all three dimensions of device structure, the precise optical modeling of the solar cells on textured substrates should be carried out using at least two-dimensional (2-D) modeling. But, this rigorous treatment requires enormous computation facilities and so a semi-empirical approach is usually chosen. Different groups have addressed this problem by more or less sophisticated semi-empirical models. Among them, the scientists who attempted this first, were Yablonovitch [48] and Cody [49]. This group was followed by Deckman *et al* [50] and Shade and Smith [51].

An original semi empirical optical model for simulating the optical properties of solar cells had been developed at the Laboratoire de Physique des Interfaces et des Couches Minces (LPICM), Ecole Polytechnique, France, by Leblanc *et al* [52–54]. In this model diffuse reflectances and transmittances due to interface roughness are derived from angular-resolved photometric measurements, and are used as input parameters to the numerical program. The electromagnetic field's specular reflection and transmission coefficients are assumed to be proportional to the classical Fresnel coefficients, the proportionality factor depending on the amount of total diffused light. Consequently specular light coherence is kept and specular interferential effects, which may be observed experimentally with a flat or even a moderately rough TCO substrate, are taken into account. However,

phase coherence between the diffused light at a rough interface and the incident light is assumed to be lost, so that diffused light effectively behaves as a new source of light; which again is partly diffused and partly specularly transmitted or reflected at a rough interface. The method is to calculate the total Poynting vector flux (due to the direct incident, specularly reflected and diffused light) at the entrance and exit points of each layer; thus obtaining the amount of light absorbed in each. Moreover, the mathematical treatment of the optical model permits one to consider normal or oblique incidence of the impinging light. The model yields the amount of light absorbed in each layer of a stacked structure (including the TCO and the metal contacts) and estimates the percentage of light reflected from the front surface of the device (optical reflection loss).

Another approach to integrated optical and electrical modeling was taken by Rubinelli *et al* [55]. For heterojunctions having textured TCO as the front contact, the generation rate profile was calculated by a light ray tracking optical modeling, accounting for light scattering at rough interfaces. A light beam in a medium, propagating into the next medium was split at the interface into a transmitted and a reflected ray. The complex reflected and transmitted waves were given by the standard Fresnel's equations. These two rays were tracked by the computer until the next interface was reached and this procedure was repeated till the ray amplitude became negligible. This process is performed on all other rays until tracking of new rays no longer alters the calculated average absorbance.

Chatterjee *et al* [56] integrated the optical model of Leblanc *et al* [54] described above into a global electrical-optical model, capable of simulating the properties of the present day state-of-the-art solar cell or any other opto-electronic device in its entirety. The model takes into account both specular interference effects and diffused reflectance and transmittance due to a rough textured surface. In amorphous semiconductor devices, the electric field is highly non-uniform on account of carrier trapping in the large number of gap states, especially under illumination. Hence calculation of the total light absorbed in each layer of the cell is not enough to study in detail the transport properties as a function of position in the device. Thus, in order to calculate accurately both the non-uniform light absorption and the extremely non-uniform field inside an amorphous device, in this model, any semiconductor device structure is subdivided into a large numbers of (typically 400 to 1000) grid points. The

light absorbed in each layer (as well as the reflection loss from the device) is obtained by taking the difference of the Poynting's vector flux from the top and bottom interface of each layer as already stated. A maximum of two rough interfaces have been considered in the model. This electrical-optical model will be described in detail later.

Several other semi-empirical 1-D optical models based on thin-film optics have been developed [57,58]. These models use the average scattering data of the rough interfaces in a-Si:H solar cells which can be determined experimentally. The model developed by Tao *et al* computes reflection and transmission at each interface of a multi-layer structure by using the Fresnel's coefficients that is only specular reflection or transmission is taken into account. Only normal incidences of the light can be modeled and scattering at the surfaces is not taken into account. This model was later improved [59] to take into account scattering due to textured substrates and in its final form is similar in approach to the model of Leblanc *et al* [54], with the added advantage that any number of rough interfaces may be considered. This model has also been integrated into a combined electrical-optical model [60]. An excellent review of electrical modeling, optical modeling and the electrical-optical modeling approach is given by Schropp and Zeman [61]

4. Dynamic inner collection efficiency in a-Si:H based PIN solar cells

In order to improve the conversion efficiency of amorphous silicon based solar cells, various analyses of the solar cell photovoltaic characteristics have been carried out. One important analysis that is necessary to improve the device design is to calculate the depth profile of the photo-generated carrier collection efficiency in the solar cell. We will then be in a position to *PIN*-point in exactly which region of the device (*e.g.* *P/I* interface, *I*-layer, *N/I* interface, *etc.*) the photo-generated carriers are mainly being lost. Takahama *et al* [62] first developed such an analysis for the calculation of the dynamic inner collection efficiency (DICE) in amorphous silicon solar cells. This quantity is defined as the probability that an electron-hole pair generated at a certain depth x inside the solar cell is collected, in other words, that it contributes to the external solar cell current. $DICE(x)$ therefore represents the depth profile of the carrier collection efficiency within the solar cell.

The first calculation of DICE by Takahama *et al* [62]

for hydrogenated amorphous silicon (a-Si:H) *PIN* solar cells made use of quantum efficiency (QE) experiments, where the current generated by a monochromatic light impinging on the cell, under a given bias light and bias voltage, is measured. This method involves calculating the inner collection efficiency at a certain depth x_j , *viz.*, $DICE(x_j)$, $j = 1, 2, \dots, m$, in a *PIN* solar cell, using the measured normalized external collection efficiency, $\eta(E_i)$, $i = 1, 2, \dots, n$, where E is the incident photon or electron energy, through a rectangular matrix, g of elements, $g_{ij} = g(E_i, x_j)$ as :

$$\eta = gDICE. \quad (2)$$

Solving this equation for DICE, requires in principle inversion of the matrix g (therefore, for the matrix g to be invertible) and for m to be equal to n . However, approximate solutions can be found for the over-determined case $m < n$ as also for the underdetermined case $m > n$, using the Singular Value Decomposition (SVD – Takahama *et al*, [62]) technique. In a typical solar cell however, DICE should be calculated at a large number of points (m) in the device because under operating illumination conditions, the electric field is strongly position dependent. Since in QE experiments, appreciable response from an a-Si:H based solar cell is obtained only over a wavelength range spanning from $0.35 \mu\text{m}$ to $0.75 \mu\text{m}$, m is in fact much larger than n . Thus the solution attempted *via* the SVD technique, has resulted in oscillatory and unstable solutions [63,64].

To improve the resolution in the standard DICE approach in the back and middle of the *I*-layer, Fischer [63] introduced the 'bifacial DICE analysis', where the combined quantum efficiency measured from the *P*-side and that measured from the *N*-side are used to generate the *I*-layer DICE profile. This analysis requires the solar cell to be contacted with a transparent conducting oxide back contact, so that light can also be made to enter the device from the back. The drawback is that this is not the case in a solar cell for optimized performance, so that the DICE calculated by this method, does not represent the DICE of a solar cell under optimal operating conditions.

Electron beams too can be used as probe instead of a probe monochromatic light, and the electron beam induced current (EBIC) technique at variable electron beam energy, has also been used to calculate the inner collection efficiency in a-Si:H based devices [65]. In this method, electron-hole pair generation in the material

takes place under the influence of an electron beam of energy E , and beam current I_b . The EBIC technique also relies on matrix inversion (inversion of eq. (2) above). However, its advantage over the photo-current generation method lies in the fact that this generation function exhibits a maximum, the position of which increases with E . It can be shown, that this leads to an easier numerical inversion. However, a weakness of this method [65] is the uncertainty in the value of the electron-hole pair generation function.

These techniques belong to the ‘inverse problem solving’ approach, in the sense that one tries to calculate DICE from the external collection efficiency *via* a matrix inversion. It was shown for the first time by Chatterjee’s group [66], that DICE or the position-dependent inner carrier collection efficiency or PDICE, as the quantity has been named hereafter, can also be calculated using a detailed electrical-optical model. This involves extracting the parameters characterizing a given solar cell, by simulating its experimentally measured J - V and QE characteristics under various conditions using a detailed electrical-optical model based on the solution of the Poisson’s and the continuity equations. These parameters can then be used *via* the ‘direct problem solving’ approach, that will be described in Section 5.3, to calculate the PDICE profile under given bias illumination and voltage conditions.

5. Description of such a typical detailed one-dimensional electrical-optical model (ASDMP)

The model that will be described in detail is the one developed by Chatterjee and named ‘Amorphous Semiconductor Device Modeling Program (ASDMP)’ [30, 31,56]. It is a versatile model, capable of simulating both the electrical and optical properties of a solar cell; in brief the functioning of a solar cell in its entirety. The electrical part consists of a detailed *ab initio* computer model capable of simulating the dark and the illuminated current density-voltage (J - V) characteristics and the quantum efficiency of the devices, in the process analyzing the electric field, carrier transport, recombination and trapping in the gap states as a function of position in the device. The program used here is applicable to a general n -layer device where the material properties vary with position and the gap state properties with both position and energy. The different layers may be amorphous, microcrystalline or polycrystalline. The model helps to analyze the role of the defects and their impact on the

overall operation of the device. It also plays an important role in providing valuable feedback for device optimization. By helping to provide the necessary directions, it also cuts down on the time spent on costly and time-consuming experiments.

This electrical model has been integrated [32] with an optical model [54] which takes into account both specular interferential effects and diffused reflection and transmission due to a rough interface. The latter is very important when a solar cell is deposited on a rough textured transparent conducting oxide (TCO) to enhance light trapping in the device. Besides solar cells, the model has also been successfully applied to semiconductor detector structures [67], temperature sensors [34] and color sensors [35].

5.1. Electrical model :

In the electrical part of the model, three coupled differential equations : the Poisson’s equation and the two carrier continuity equations. are solved simultaneously under non-equilibrium steady state conditions (*i.e.* under the effect of voltage or light bias, or both), directly from the first principles. The equations used are :

Poisson’s equation :

$$\frac{\partial^2 \Psi(x)}{\partial x^2} = \frac{\rho(x)}{\epsilon} \quad (3)$$

Hole continuity equation :

$$0 = G(x) - R(p(x), n(x)) - \frac{1}{q} \frac{\partial J_p(x)}{\partial x} \quad (4)$$

Electron continuity equation :

$$0 = G(x) - R(p(x), n(x)) + \frac{1}{q} \frac{\partial J_n(x)}{\partial x} \quad (5)$$

where $\rho(x)$ = net charge density

$$= q \left[p(x) - n(x) + p_T(x) - n_T(x) + N_{\text{net}}^+ \right] \quad (6)$$

and the electric field

$$E = \frac{\partial \Psi(x)}{\partial x} \quad (7)$$

Here, ϵ is the dielectric constant, E the electrostatic field, $\Psi(x)$ represents the position in energy of the local vacuum level, x the position in the device, p and n the valence-band hole density and the conduction band electron density respectively, q the electronic charge, R the recombination rate, p_T and n_T the trapped hole and

electron population density respectively, N_{net}^+ the net doping density, if any, G the electron-hole pair generation rate, J_p and J_n the hole and electron current density respectively and E_{F_p} and E_{F_n} the hole and electron quasi-Fermi levels. In our calculations, the three state variables that completely define the state of a device have been taken to be the local vacuum level, ψ , and the quasi-Fermi levels E_{F_p} and E_{F_n} . Once these three dependent variables are known as a function of x , all other information about the system can be determined as functions of position. In thermodynamic equilibrium, the Fermi level is a constant as a function of position, and hence the three eqs. (3)–(5) essentially reduce to only one equation. *viz.*, the Poisson's equation. This is a second order non-linear differential equation, with one dependent variable, local vacuum level $\psi(x)$ and one independent variable (x). This equation must be solved subject to the boundary conditions

$$\psi(0) = 0 - \chi(L) - \phi_{BL} + \phi_{B0} + \chi(0) \quad (8a)$$

and

$$\psi(L) = 0 \quad (8b)$$

in thermodynamic equilibrium. Once $\psi = \psi(x)$ is obtained, the band edges, fields, free carrier populations and trapped charges present at thermodynamic equilibrium are found.

In the non-thermodynamic equilibrium steady-state, a system of three coupled non-linear second order differential equations in the three unknowns (ψ, E_{F_n}, E_{F_p}) are obtained. In order to solve these equations for our state variables (ψ, E_{F_n}, E_{F_p}), we need six boundary conditions, two for each dependent variable. The two boundary conditions used in non-thermodynamic equilibrium are modified versions of (8a) and (8b)

$$\psi(0) = 0 - \chi(L) - \phi_{BL} + \phi_{B0} + \chi(0) - V \quad (8c)$$

and

$$\psi(L) = 0, \quad (8d)$$

where L is the length of the device, $\chi(0)$, $\chi(L)$ are the electron affinities at $x = 0$ and $x = L$ respectively and V is the externally applied voltage, ϕ_{b0} and ϕ_{BL} are the distances in energy from the Fermi level to the conduction band in thermodynamic equilibrium. It should also be mentioned here that $\psi = \psi(x) = 0$ is chosen to be the position in energy of the vacuum level at the boundary point $x = L$.

The four other boundary conditions are obtained from imposing constraints on the currents at the boundaries at

$x = 0$ and $x = L$. These constraints force the mathematics to acknowledge the fact that the currents must cross at $x = 0$ and $x = L$ (the contact positions) by either thermionic emission or interface recombination. Expressed mathematically, we obtain the followings :

$$J_n(0) = qS_{n0} [n(0) - n_0(0)], \quad (9a)$$

$$J_p(0) = -qS_{p0} [p(0) - p_0(0)], \quad (9b)$$

$$J_n(L) = -qS_{nL} [n(L) - n_0(L)], \quad (10a)$$

$$J_p(L) = qS_{pL} [p(L) - p_0(L)], \quad (10b)$$

where S_{n0}, S_{p0} are surface recombination velocities for electrons and holes respectively at the $x = 0$ interface, and the quantities S_{nL}, S_{pL} are the corresponding velocities at the $x = L$ interface. The largest value they can have is $\sim 10^7$ cm/sec dictated by thermo-ionic emission. Here $n(0)p(0)$ are the electron (hole) density at $x = 0$, $n(L)p(L)$ are the same at $x = L$. $n_0(0)p_0(0)$, $n_0(L)p_0(L)$, are the electron (hole) density in the thermodynamic equilibrium at $x = 0$ and $x = L$ respectively. The quantities $\phi_{B0}, \phi_{BL}, S_{n0}, S_{p0}, S_{nL}$ and S_{pL} are the six boundary conditions that determine the quality of the contacts to the solar cell or the semiconductor device under study. By varying these one can change the degree of ohmicity of the contacts. With the help of the boundary conditions stated above, the three equations (3) to (5) can be solved simultaneously for $\psi = \psi(x)$, $E_{F_n} = E_{F_n}(x)$ and $E_{F_p} = E_{F_p}(x)$. For this, the different terms in the equations are to be calculated first. This is discussed below.

5.1.1. Calculation of the net charge density :

The net charge density $\rho(x)$ can be represented by eq. (6) :

$$\rho(x) = q [p(x) - n(x) + p_T(x) - n_T(x) + N_{\text{net}}^+],$$

where $p(x)$ is the number of valence band holes per unit volume, $n(x)$ is the number of conduction band electrons per unit volume, $p_T(x)$ = number of trapped holes per unit volume arising from continuous localized states, $n_T(x)$ = number of trapped electrons per unit volume arising from continuous localized states, N_{net}^+ = net effective discrete localized state density, which may be the impurity trapped charge in the case of doped semiconductors.

A. Free carrier population model :

Calculation of free charges in thermodynamic equilibrium :

The models for the n and p terms of eq. (6) are developed assuming the very general band structure seen in Figure 1. Here $\psi = \psi(x)$ gives the value of the vacuum

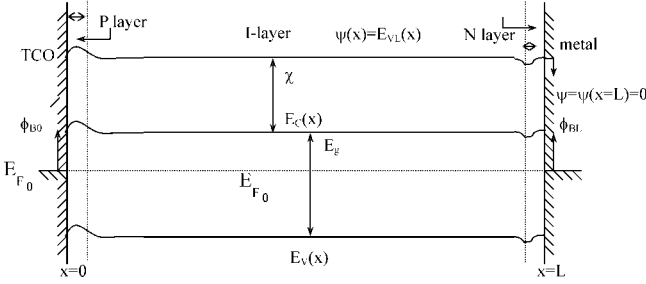


Figure 1. Band diagram of a PIN junction cell in thermodynamic equilibrium.

level E_{vL} at some point x .

The free-hole density at thermodynamic equilibrium

$$p_0(x) = N_v(x) \exp\left[-\frac{E_{F_0} - E_v(x)}{kT}\right]. \quad (11)$$

From the definitions,

$$E_{F_0} = \psi(L) - \chi(L) - \phi_{BL}$$

or

$$E_{F_0} = 0 - \chi(L) - \phi_{BL}. \quad (12)$$

Also

$$E_v(x) = \psi(x) - \chi(x) - E_g(x) \quad (13)$$

From eqs. (12) and (13), (11) becomes

$$p_0(x) = N_v(x) \exp\left[-\frac{0 - \chi(L) - \phi_{BL} - \psi(x) + \chi(x) + E_g(x)}{kT}\right]. \quad (14)$$

Similarly, free electron density,

$$n_0(x) = N_c(x) \exp\left[-\frac{E_c(x) - E_{F_0}}{kT}\right]. \quad (15)$$

Thus, eqs. (14) and (15) give the required expressions for the free hole and electron densities in thermodynamic equilibrium.

Free charges at non-thermodynamic equilibrium steady-state :

Here, the Fermi level splits up into two quasi-Fermi levels E_{Fn} and E_{Fp} . Therefore, the expressions for the

free holes and the free electrons take the following forms :

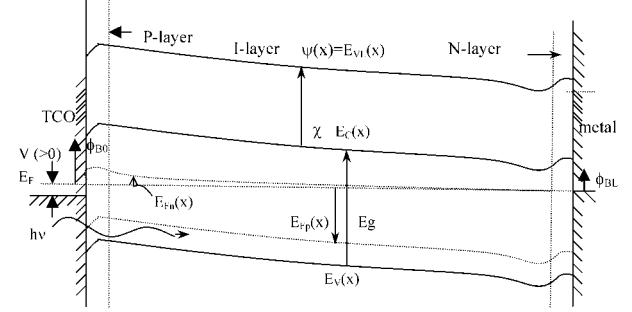


Figure 2. Band diagram of a PIN junction cell under voltage and illumination bias.

$$p(x) = N_v(x) \exp\left[-\frac{E_{Fp}(x) - E_v(x)}{kT}\right] \quad (16)$$

and

$$n(x) = N_c(x) \exp\left[-\frac{E_c(x) - E_{Fn}(x)}{kT}\right], \quad (17)$$

where p and n are the hole and electron densities in non-thermodynamic equilibrium steady state.

B. Discrete localized state model :

Discrete localized states include states arising from an intentional introduction of impurities (doping) or from unintentional discrete impurity or defect states. In any case, the charge arising from these discrete states can be expressed as

$$N_{net}^+ = N_D^+ - N_A^- \quad (18)$$

where N_D^+ , the number of charged donor-like states per volume in a particular layer and N_A^- , the number of charged acceptor-like states per volume in the same layer, are determined by the discrete state concentrations and ionization energies. Two options may be used here (i) full ionization and (ii) partial ionization. If full ionization is assumed, then N_D and N_A are treated as donor and acceptor sites that fully ionize such that $N_D^+ = N_D$ and $N_A^- = N_A$.

At present, only fully ionized discrete states exist in our non-equilibrium model. Therefore, N_{net}^+ is simply $N_D - N_A$, where N_D and N_A are the donor and acceptor impurity concentrations, respectively.

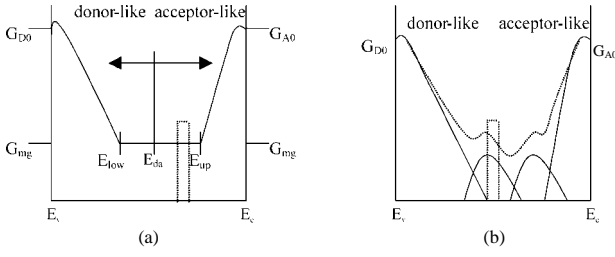


Figure 3. Typical gap-state distributions used in program ASDMP : (a) U-shaped model, where a constant distribution of midgap states (G_{mg}) is assumed and (b) where the midgap states are modeled using two Gaussian distribution functions. In both cases, donor-like and acceptor-like tail states with exponential prefactors G_{D0} and G_{A0} are present. The dotted line represents the typical net DOS in (b). The bar indicates a possible discrete localized state DOS. E_{da} is the energy at which the states change from a donor-like to an acceptor-like nature.

C. Continuous localized state model :

Continuous localized states are those localized states that form a continuum throughout the bandgap. These continuum gap states are to be distinguished from the discrete localized states, discussed above, which only exist at specific energies in the energy gap. In amorphous or disordered semiconductors, for which class of materials this model has been primarily set up, such a quasi-continuum of states exists in the mobility gap.

(i) Distribution :

The symbol $p_T(x)$ denotes the total number of continuum, donor-like gap states per volume that are ionized at a point x . These unwanted donor-like continuum states are usually concentrated in the lower half of the bandgap in amorphous materials and they generally lose their electron to the valence band, hence p_T represents the trapped holes per unit volume. Similarly, acceptor-like continuum states are concentrated in the upper half for a-Si:H based materials. These gain their electrons from the conduction band and hence n_T is the number of trapped electrons per unit volume in these states. Before computing p_T and n_T , the model used for distribution of the gap states is described. Figure 3 gives the two different types of gap state distribution incorporated in our modeling program.

(a) Tail state distribution :

In both models, we have donor-like states ($D^{+/0}$) coming out of the valence band and acceptor-like states ($D^{-/0}$) coming out of the conduction band.

This consists of: the Urbach tail of donor-like states coming out of the valence band are modeled by :

$$g_{DT}(E) = G_{D0} \exp[-E/E_D]; \quad E \text{ measured from } E_v. \quad (19)$$

The Urbach tail of acceptor-like states coming out of the conduction band are modeled by :

$$g_{AT}(E') = G_{A0} \exp[-E'/E_A]; \quad E' \text{ measured from } E_c, \quad (20)$$

where g is the density of states (DOS) per cc per eV and G_{D0} (G_{A0}) are the exponential prefactors ($\text{cm}^{-3} \text{eV}^{-1}$) of the respective Urbach tails. E_D , E_A are the characteristic energy of the valence and conduction band tails respectively.

(b) Mid-gap states (dangling bond defects) distribution:

U-shaped distribution :

Here, the density of midgap states is equal to a constant value, G_{mg} (as seen in Figure 3a). Measuring E positively down from E_c , we note that this flat region extends from $E = E_{up}$ to $E = E_c - E_{low}$, where E_{up} and E_{low} are positive numbers defined as

$$E_{up} = E_A \cdot \ln(G_{A0} / G_{mg}), \quad (21)$$

$$E_{low} = E_D \cdot \ln(G_{D0} / G_{mg}). \quad (22)$$

The quantity E_{up} is measured positively down from E_c and the quantity E_{low} is measured positively up from E_v . These midgap states are assumed to be acceptor-like ($D^{-/0}$) for $((E - E_c) < E_{da})$, and donor-like ($D^{+/0}$) for $((E - E_c) > E_{da})$. For this reason, E_{da} is called the switchover energy, and is measured positively down from the conduction band edge E_c . This flat region is then added to the exponential region, thus completing the U-shaped model.

Gaussian distribution of midgap states :

Here, the midgap states have been modelled using two Gaussian distribution functions. In the case of hydrogenated amorphous silicon (a-Si:H), the separation between peaks of Gaussian distribution functions has been assumed to be 0.5 eV. The reason for choosing 0.5 eV as the correlation energy, is to have a trough in the net DOS between the Gaussian peaks. This has been observed by subgap absorption [68] and photoconductivity [69] experiments. The upper Gaussian is composed of acceptor-like ($D^{-/0}$) states (density $N_{AG} \text{ cm}^{-3}$), while the lower one, consists of donor-like ($D^{+/0}$) states (density $N_{DG} \text{ cm}^{-3}$). The expressions for the DOS in the two cases are given by :

$$g_{AG}(E'') = \left(\frac{N_{AG}}{\sqrt{2\pi}\sigma_{AG}} \right) \exp \left\{ -\frac{(E'' - E_{AG})^2}{2\sigma_{AG}^2} \right\}, \quad (23)$$

$$g_{DG}(E''') = \left(\frac{N_{DG}}{\sqrt{2\pi}\sigma_{DG}} \right) \exp \left\{ -\frac{(E''' - E_{DG})^2}{2\sigma_{DG}^2} \right\} \quad (24)$$

where $N_{AG}(N_{DG})$ is the total DOS per cc in the acceptor (donor) Gaussian; $E_{AG}(E_{DG})$ is the position in eV of the peak of the acceptor (donor) Gaussian measured from the conduction (valence) band edge; $\sigma_{AG}(\sigma_{DG})$ is the respective standard deviation of the Gaussian and the energies E'' and E''' are measured respectively from the peak (E_{AG}) of the acceptor-like Gaussian distribution and the peak (E_{DG}) of the donor-like Gaussian distribution. In the region of overlap between the Gaussian distribution functions, both donor-like and acceptor-like states exist. However, the amphoteric nature of the deep dangling bond states has not been taken into account.

Midgap state distribution calculated on the basis of the defect pool model :

Since the energy of the dangling-bond states can take a range of values, due to the inherent disorder of the amorphous network, then proper consideration of the chemical equilibrium model leads to an energy shift of the peak of the formed defects, due to the minimization of free energy. Furthermore, this energy shift is different for defects formed in the different charge states (+, 0, -). This is the so-called defect-pool model [70-72]. This model allows for the probability of a dangling bond being formed in each of the three charged states (+, 0, -), thus taking into account the amphoteric nature of a dangling bond defect.

The genesis of the defect-pool model lies in the work of Bar-Yam and Joannopoulos [73] who first pointed out that the formation energy of a defect depends on its charge state and that the difference in the formation energies depends on the Fermi energy and the energy of the defect itself.

Stutzmann [74] introduced the weak-bond dangling-bond conversion model and Smith and Wagner [75] identified the weak-bond energies with the valence-band-tail states, which are exponentially distributed in energy, giving a further distribution of formation energies.

Winer brought together these different aspects in a

classic paper, which defined the modern defect-pool model [76]. He calculated the density of states in undoped and doped a-Si:H and produced the key result that for a sufficiently wide pool, negatively charged defects in N -type material were lower in energy than positively charged defects in P -type material, even when the correlation energy is positive. This surprising result, found in many experiments [68,77,78] could not be explained on the basis of fixed Gaussian distribution functions representing dangling bond defects.

Powell and Deane [79,80] have presented a modified defect-pool model, where they have shown that the energy spectrum of the density of states does depend on the number of Si-H bonds mediating the weak bond breaking reaction, and that on this basis it is possible to calculate, analytically, the density-of-states distribution. They have concluded that the best agreement with experimental results is obtained for a rather wide defect pool and for a model where two Si-H bonds mediate the weak-bond breaking reaction. Using data from a wide range of experiments, they have calculated a density-of-states distribution for intrinsic a-Si:H with approximately four times as many charged defects as neutral ones.

The defect-pool model for calculating the density of dangling bond defects in hydrogenated amorphous silicon, has not yet been incorporated into ASDMP.

(ii) Probability of occupation function :

As already mentioned, in amorphous semiconductors, a quasi-continuum of states exists in the mobility gap. Their distributions, as assumed in this model, has been described in the previous section. Here, therefore the total number of trapped holes per cc (p_T) must be computed by integrating the trapped charges in all the donor-like states. Likewise, n_T , the total number of trapped electrons per cc, is computed by integrating the trapped charges in all the acceptor-like states. It may be pointed out here, that we have assumed all states to be singly charged states. In other words, a donor-like state is defined as one having a single positive charge when empty, and is neutral (has zero charge) when filled with an electron. An acceptor-like state has a single negative charge when occupied by an electron, and is neutral when empty. In order to calculate the values of p_T and n_T in both thermodynamic equilibrium and in the non-thermodynamic equilibrium steady state, we need first to

consider the probability of occupation function.

Thermodynamic equilibrium probability of occupation function :

The usual Fermi-Dirac distribution function :

$$f_0 = \frac{1}{1 + \exp\left[\frac{(E_t - E_{F_0})}{kT}\right]} \quad (25)$$

represents the probability of electron occupation of a state. The probability of hole occupation is given by $(1 - f_0)$. In the above equation E_t is the position on the energy scale of a defect level in the mobility gap, E_{F_0} is the thermodynamic equilibrium Fermi level and T the ambient temperature.

Non-thermodynamic equilibrium steady state probability of occupation function :

In order to arrive at the expression of this probability function, we have made use of the Shockley-Read-Hall model and considered the following four processes responsible for populating and depopulating a particular defect state N_t in the mobility gap : (a) electron emission e_n , (b) electron capture c_n , (c) hole emission e_p and (d) hole capture c_p

where

$$e_n = a_n f N_t, \quad (26a)$$

$$c_n = n(1 - f)N_t \sigma_n v_{th}, \quad (26b)$$

$$e_p = a_p (1 - f)N_t, \quad (26c)$$

$$c_p = pfN_t \sigma_p v_{th}, \quad (26d)$$

where $\sigma_n(\sigma_p)$ is the capture cross-sections of electrons (holes) in the states $N_t \text{ cm}^{-3}$, v is the thermal velocity and a_n and a_p are constants to be determined using the law of detailed balance in thermodynamic equilibrium, f is the probability of occupation function. For any steady state condition, the following equation holds :

$$c_n - e_n = c_p - e_p = R, \quad (27)$$

where R is the recombination rate in $\text{cm}^{-3} \text{ sec}^{-1}$.

In thermodynamic equilibrium, $R = 0$ and we have

$$c_n - e_n = c_p - e_p = 0. \quad (28)$$

In thermodynamic equilibrium, using $f = f_0$ (eq. (25)) and $e_n = c_n$, we obtain from eqs. (26a) and (26b)

$$a_n = n_0 \frac{(1 - f_0)}{f_0} \sigma_n v_{th}, \quad (n = n \text{ in thermodynamic equilibrium}).$$

$$= \sigma_n v_{th} n_1; \quad n_1 = N_c \exp\left[-\frac{(E_c - E_t)}{kT}\right]. \quad (29)$$

Similarly using $f = f_0$ and $e_p = c_p$, we obtain from eqs. (26c) and (26d)

$$a_p = p_0 \left(\frac{f_0}{1 - f_0} \right) \sigma_p v_{th}, \quad (p = p_0 \text{ in thermodynamic equilibrium}).$$

$$= \sigma_p v_{th} p_1; \quad p_1 = N_v \exp\left[-\frac{(E_t - E_v)}{kT}\right]. \quad (30)$$

In the above, $n_0(p_0)$ is the free electron (hole) population in thermodynamic equilibrium and $N_c(N_v)$ the effective DOS in the conduction (valence) band. Substituting the expression of a_n (eq. (29)) and a_p (eq. (30)) in eq. (26), we obtain, using the law of detailed balance (eq. (27)), the expression for the probability of occupation function f in the steady state condition under voltage or light bias as

$$f = (\sigma_n n + \sigma_p p_1) / [\sigma_n (n + n_1) + \sigma_p (p + p_1)], \quad (31)$$

where $n(p)$ are the free electron (hole) population in the non-equilibrium steady state. In calculating the above expression for the occupation function, we have correctly accounted for the temperature effect, *i.e.* the Taylor-Simmons [16] approximation ($T = 0^\circ\text{K}$) has not been used in the present analysis.

(iii) *Charge in localized states :*

We obtain p_T and n_T , the trapped hole and electron densities in the localized gap states by integrating the product of the localized gap state density and the occupation function across the mobility gap. We do this by dividing the energy gap into a large number of intervals, assuming the density of states per energy, G_t to be constant in each tiny energy interval $[E_1, E_2]$. G_t is the value of the DOS at the midpoint of the energy interval, calculated using the various distributions, described in part (i) of the present Section 'Continuous localized state model'.

Thermodynamic equilibrium trapped charges :

For a band of donor states in the energy region $[E_1, E_2]$ with constant DOS per energy $G_t = G_D$ the trapped hole population is given by :

$$p_t = G_D \int_{E_1}^{E_2} (1 - f_0(E)) dE, \quad (32)$$

where f_0 is the thermodynamic equilibrium probability of occupation function, given in eq. (25).

Similarly, for a band of acceptor states in the energy region $[E_1, E_2]$ with constant DOS per energy $G_t = G_A$, the trapped electron population is given by :

$$n_t = G_A \int_{E_1}^{E_2} f_0 dE. \quad (33)$$

Trapped charges at the steady state under voltage and/or light bias :

Here again, for a band of donor states in the energy interval.

Here again, for a band of donor states in the energy interval $[E_1, E_2]$ with constant DOS per energy $G_t = G_D$, the trapped hole population is given by :

$$p_t = G_D \int_{E_1}^{E_2} (1 - f) dE, \quad (34)$$

where f is the probability of occupation function in the non-equilibrium steady state given by eq. (31).

Likewise,

$$n_t = G_A \int_{E_1}^{E_2} f dE, \quad (35)$$

where G_A is the constant density of acceptor-like states in the energy interval $[E_1, E_2]$.

5.1.2. Recombination through localized states :

The recombination term, R appears in the continuity eqs. (4) and (5). To develop the equation for the recombination traffic through the gap states we use the Shockley-Read-Hall model using the expression (27) for the recombination R we obtain

$$R = c_n - e_n = (c_p - e_p) \quad (36)$$

where f is the probability of occupation function under non-equilibrium steady state conditions, and is given by eq. (31). The above expression is obtained by substituting the value of a_n in eq. (29) in the expression for e_n (eq. (26a)) and also using the expression (26b) for c_n . Substituting for f from eq. (31) and simplifying, we obtain

$$R(\text{cm}^{-3} \text{sec}^{-1}) = \sigma_n \sigma_p v_{th} N_t \left[\frac{np - n_i^2}{\sigma_n (n + n_1) + \sigma_p (p + p_1)} \right], \quad (37)$$

where n_i , the intrinsic carrier density is given by

$$n_i = \sqrt{N_c N_v} \exp \left[\frac{-E_g}{2kT} \right], \quad (38)$$

$$[E_g = E_c - E_v].$$

For a band of states ($N_t \text{ cm}^{-3}$) in the energy region $[E_1, E_2]$ with a constant DOS per energy G_t , the expression for recombination becomes :

$$R = \sigma_n \sigma_p v_{th} G_t \int_{E_1}^{E_2} \left[\frac{np - n_i^2}{\sigma_n (n + n_1) + \sigma_p (p + p_1)} \right] dE. \quad (39)$$

5.1.3. Expressions for J_n, J_p :

Current density terms J_p, J_n appear in the continuity eqs. (4) and (5). From transport theory, these have been expressed as :

$$J_p(x) = qp\mu_p \nabla E_{F_p}, \quad (40)$$

$$J_n(x) = qn\mu_n \nabla E_{F_n}. \quad (41)$$

Here $\mu_n (\mu_p)$ are the electron (hole) band microscopic mobility, $E_{F_n} (E_{F_p})$ – the quasi-Fermi level for electron (hole) and q – the electronic charge.

The equation for J_n and J_p can be expressed as

$$J_n = qn\mu_n \nabla(\psi - \chi) + qD_n \nabla n - qnD_n \nabla(\ln N_c), \quad (42)$$

$$J_p = qp\mu_p \nabla(\psi - \chi - E_g) - qD_p \nabla p + qpD_p \nabla(\ln N_v), \quad (43)$$

where ψ is the vacuum level, χ is the electron affinity, $D_n(D_p)$ – the electron(hole) diffusion constant, and $N_c(N_v)$ – the effective DOS in the conduction (valence) band. Here, term 1 is the drift due to the ‘effective field’ on the electrons (holes), which in a hetero-junction ($\nabla\chi \neq 0$) includes besides the usual electrostatic field, also a contribution due to the gradient in the electron affinity. In other words, term 1 includes the gradient of the conduction (valence) band edge $E_c(E_v)$. For a homo-junction, $\nabla\chi = 0$ and hence, the first term reduces to ψ only. Term 2 is the usual diffusion term due to the carrier concentration gradient, while the last term determines the diffusion due to the gradient (if any) in the number of available states $N_c(N_v)$ per cm^3 in the

conduction (valence) band.

5.2. Calculation of dark reverse bias current taking into account high field emission under reverse bias conditions :

In any type of detector structure, the dark reverse bias current is detrimental to device performance. That is why it is very important to have the minimum possible value for the dark reverse bias leakage current. The possible origins of this leakage current are bulk thermal generation, contact injection and edge leakage. It has been demonstrated that for PIN structures with doped layers that provide good blocking contacts, the contact injection currents are negligible; hence the dark reverse bias leakage currents are controlled by thermal generation of electron-hole pairs through the bulk defect states. It was demonstrated [81,82] that the reverse bias current is strongly influenced by the high electrical field existing in a diode under reverse bias. These authors suggested that field-enhanced thermal generation takes place under reverse bias conditions, and introduced this effect in their simulation model AMPS *via* a Poole-Frenkel mechanism. Similar modifications have been introduced in the model ASDMP of P Chatterjee, who demonstrated that the reverse bias dark current is enhanced by nearly three orders of magnitude in the case of a thin ~600 nm diode. The high field enhancement (HFE) effect was originally suggested by Poole [83,84] and later modified by Frenkel [85]. It basically enhances the population of a band in the presence of an electric field. Let us consider a donor-like localized gap state, which is characterized by a long-range Coulombic attraction for electrons. Then in the presence of an electric field ξ , the superposition of the Coulomb potential of the donor-like site and the potential of the electric field results in the lowering of the ionisation energy of the donor-like site by an amount ϕ_m . If the donor-like sites are far enough apart that their Coulomb potentials do not overlap, as we assume to be the case here, then [86,87]

$$\phi_m = \beta \xi^{1/2}. \quad (44)$$

In this equation,

$$\beta = [q / (\pi \epsilon)]^{1/2}, \quad (45)$$

where ϵ is the material permittivity and q the electronic charge. The conductivity of the conduction band is then

enhanced by the factor

$$\exp(\beta \xi^{1/2} / kT), \quad (46)$$

where k is the Boltzmann's constant and T – the absolute temperature. This is the Poole-Frenkel effect that enhances the thermal generation in the presence of an electric field. It was only after this modification in the program was made, that we could correctly reproduce the experimentally measured reverse bias currents from PIN diodes having standard hydrogenated amorphous silicon and polymorphous silicon *I*-layers.

5.3. Calculation of the position-dependent inner carrier collection efficiency (PDICE) in solar cells :

Position dependent inner carrier collection efficiency $PDICE(x_i)$ has been calculated as follows: The PIN cell is divided into a large number of segments (typically 600), so that the calculated PDICE may be sensitive to the internal electric field, under a given bias light (BL) and voltage V . BL is assumed to enter through the *P*-layer, and the start of this layer is designated as $x = 0$. For the purpose of calculating PDICE at x_i , we produce with the help of our model, generation of BL in all the 600 segments, and additional $G(x_i)$ generation in only the segment at x_i . Similarly for calculating $PDICE(x_{i+1})$ we produce additional $G(x_{i+1})$ generation in segment x_{i+1} . $G(x_i)$ may be produced by any light signal, but it must have a delta function position dependence, being non-zero only in the required segment x_i where $PDICE$ is being calculated. The normalized collection, $C_{p,0}(G(x_i), BL, V)$ of holes at $x = 0$, due to $G(x_i)$ at x_i is defined as :

$$C_{p,0}(G(x_i), BL, V) = \frac{[Abs(J_{p,0}\{(BL + G(x_i)), V\}) - Abs(J_{p,0}(BL, V))]/q}{G(x_i)}, \quad (47)$$

where the subscript '0' of the hole current J_p represents its value at $x = 0$ and q is the electronic charge. This collection depends on the applied BL and V . We can similarly define the normalized collection $C_{n,0}(G(x_i), BL, V)$ of electrons at $x = 0$, due to $G(x_i)$ at x_i . Then :

$$PDICE(x_i, BL, V) = C_{p,0}(G(x_i), BL, V) - C_{n,0}(G(x_i), BL, V). \quad (48)$$

The difference in the numerator of eq. (47), $\Delta J_{p,0}$, is in general, the sum of :

$$\Delta J_{p,0} = J_{p,0}(G(x_i)) + \sum_k \frac{\partial J_{p,0}(BL, V)}{\partial \xi_k(G(x_i))} \Delta \xi_k(G(x_i)). \quad (49)$$

The first term of eq. (49) is the hole current at $x = 0$ due to the generations $G(x_i)$ at x_i . The second term is the extra BL hole current at $x = 0$ (if any) due to the now well-known ‘photogating effect’ [88,89,35], where ξ_k represents different parameters, a change of which may give rise to this effect, such as the electric field, N/I potential barrier, *etc.* But for $PDICE(x_i)$ to be calculated from eq. (48), the numerator of $C_{p,0}(G(x_i), BL, V)$ should be the first term of eq. (49) alone. To minimize the effect of the second term of the eq. (49), $G(x_i)$ is chosen to be two orders of magnitude lower than the intensity of BL at x_i . Under these conditions, the second term in eq. (49) is often negligible, but when it is not, $PDICE$ has to be renamed a ‘position-dependent carrier collection response’ instead of ‘efficiency’. Also then, $PDICE(x_i)$ becomes a function of the intensity of $G(x_i)$. We would like to emphasize however, that in all experiments on QE and calculations of $PDICE$ [62,63], the modifications described by the second term of eq. (49) actually exist, and when non-negligible, can give rise to QE or $PDICE$ higher than unity. The value of $PDICE(x_i)$ calculated by eq. (48) is identical to its value from :

$$PDICE(x_i, BL, V) = C_{n,L}(G(x_i), BL, V) - C_{p,L}(G(x_i), BL, V), \quad (50)$$

where $C_{n,L}(G(x_i), BL, V)$ and $C_{p,L}(G(x_i), BL, V)$ are the normalized collection of electrons and holes respectively, at $x = L$ (the N -layer/metal back contact junction), due to the generation $G(x_i)$ at x_i .

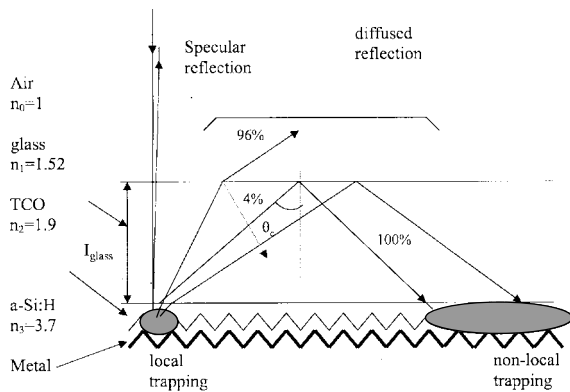


Figure 4. Propagation of light in a PIN device deposited on a rough surface : local and non-local trapping.

5.4. Generation/optical model :

In our present integrated electrical-optical modeling program, there are two options for calculating the

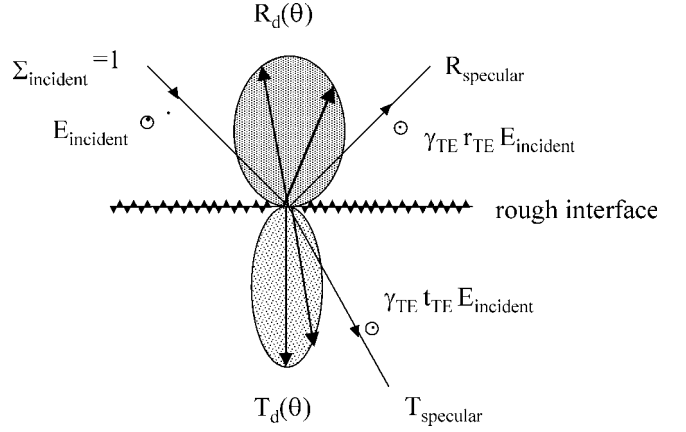


Figure 5. Schematic illustration of the assumptions of the model for the specular and diffused transmission and reflection of the TE mode. The same assumptions are made for the TM mode, where H replaces E .

generation term in the continuity equations: (i) the generation model using the exponential absorption law and (ii) the generation model which besides calculating the absorption *via* the exponential absorption law, also takes into account specular interferential effects as well as light trapping due to rough interfaces. It is this latter optical model that has been used for all calculations in this article.

(i) *Generation model using the exponential absorption law :*

Initially in this program the optical generation rate G which appears in the continuity eqs. (4) and (5), was calculated using a formula based on the simple exponential law of absorption. Here,

$$G = \sum_{\lambda} \alpha_{\lambda} \phi_{\lambda} e^{(-\alpha_{\lambda} x)} \quad (51)$$

and represents the photogeneration due to light of an arbitrary spectrum where the incident flux of each component, characterized by an absorption coefficient of α_{λ} in the material, is ϕ_{λ} . This exponential absorption law may be used for the calculation of the generation term. But, this method has several drawbacks, *e.g.* the optical losses suffered by reflection or in the transparent conducting oxide at the front contact and in the back metal contact are not considered properly. Furthermore, specular interferential effects or light trapping by diffused

reflection and transmission due to scattering at rough surfaces were not taken into account at all. Hence, an alternative method was incorporated in the program to calculate the optical generation in the device correctly. This is described below.

(ii) *Generation model taking into account specular interferential effects and light trapping due to rough interfaces :*

The generation term in the continuity equations has been calculated using an original semi-empirical model [52, 54], that has been integrated into the modeling program. Figure 4 shows the propagation of light in a *PIN* device which is deposited on a textured TCO coated glass substrate. A part of the light is specularly reflected and transmitted, while the other part undergoes diffused reflection and transmission. This is shown in more details in Figure 5. Due to the roughness of the TCO and jumps in the refractive indices between the different materials shown, two types of optical confinement take place, which may be distinguished in terms of their relative distance :

(a) Local trapping in the thin layers, due to reflection at different interfaces. This, as shown in the figure, is on a microscopic scale and takes place in the layers of the solar cell itself. The blue wavelengths are strongly absorbed in a-Si:H, and hence local trapping for such wavelengths is unimportant. However for the weakly absorbed red wavelengths $> 6000 \text{ \AA}$, such trapping is very important. The index of refraction is the highest for intrinsic a-Si:H ($n \sim 3.7$ for 6000 \AA) and decreases progressively as one passes through the *P*-layer ($n \sim 3.4$), the TCO ($n \sim 1.9$), glass ($n \sim 1.5$) and air ($n = 1$). Thus on account of total internal reflection, a considerable part of the energy reflected by the metal electrode is trapped in the active absorber a-Si:H layer.

(b) Non-local trapping, due to total internal reflection of the energy diffused by the structure at the glass/air interface, and shown in Figure 4.

We now come to a brief description of the optical model. According to the classical thin film theory, the propagation of an electromagnetic plane wave incident upon a stack of thin layers separated by ideally flat interfaces, can be solved from the classical Maxwell equations. For general non-normal incidence, the incident light is divided into two polarized modes – the transverse electric (TE) and the transverse magnetic (TM) – which are linearly polarized perpendicular to the direction of propagation, *i.e.* to the wave vector \mathbf{k} . For the TE (TM)

polarization mode, the field's amplitude reflection and transmission coefficients $r_{TE_{12}}$ and $t_{TE_{12}}$ ($r_{TM_{12}}$ and $t_{TM_{12}}$) at the interface between two layers 1 and 2 depend on the electromagnetic wave's angle of incidence. k_{xy} is the component of \mathbf{k} lying in the interface plane xy . According to the Descartes-Snell's law, k_{xy} remains constant at the reflection and refraction at each interface, and therefore is an invariant variable when specular light propagates through the entire stack. Thus, $r_{TE_{12}}$, $t_{TE_{12}}$, $r_{TM_{12}}$ and $t_{TM_{12}}$ are given as functions of k_{xy} by :

$$r_{TE_{12}} = \frac{k_{1z} - k_{2z}}{k_{1z} + k_{2z}}, \quad t_{TE_{12}} = \frac{2k_{1z}}{k_{1z} + k_{2z}}, \quad (52)$$

$$r_{TM_{12}} = \frac{\frac{k_{1z}}{\epsilon_1} - \frac{k_{2z}}{\epsilon_2}}{\frac{k_{1z}}{\epsilon_1} + \frac{k_{2z}}{\epsilon_2}}, \quad t_{TM_{12}} = \frac{2 \frac{k_{1z}}{\epsilon_1}}{\frac{k_{1z}}{\epsilon_1} + \frac{k_{2z}}{\epsilon_2}}, \quad (53)$$

where

$$k_{mz} = \left[\left(\frac{2\pi}{\lambda} \right)^2 \epsilon_m - k_{xy}^2 \right]^{1/2} \quad (m = 1, 2), \quad (54)$$

$$\text{due to } \mathbf{k}_m \cdot \mathbf{k}_m = \left(\frac{2\pi}{\lambda} \right)^2 \tilde{n}_m^2 = \left(\frac{2\pi}{\lambda} \right)^2 \epsilon_m, \quad (55)$$

where \tilde{n}_m and ϵ_m are the complex refractive index and dielectric permittivity of the medium m , and λ the wavelength in vacuum.

The total electromagnetic field at each interface of the entire stack is the sum of the components coming from multiple reflection and refraction. This total electromagnetic field may directly be derived by using the powerful matrix method of Abeles [90,91]. At a given interface between two media m and $m + 1$, in the case of TE mode (for the TM mode, the magnetic field amplitude \mathbf{H} replaces the electric field amplitude \mathbf{E}), fields propagating in both directions $E_{m,+}$ and $E_{m,-}$ in the medium m are correlated to the fields $E_{m+1,+}$ and $E_{m+1,-}$ propagating in the medium $m + 1$ by the interface matrix $I_{m/m+1}$ given by

$$I_{m/m+1} = \frac{1}{t_{TE_{m,m+1}}} \begin{pmatrix} 1 & r_{TE_{m,m+1}} \\ r_{TE_{m,m+1}} & 1 \end{pmatrix}. \quad (56)$$

Field propagation through layer m is described by a diagonal propagation matrix P_m given by

$$P_m = \begin{pmatrix} \exp(-ik_z l_m) & 0 \\ 0 & \exp(+ik_z l_m) \end{pmatrix}, \quad (57)$$

where l_m is the layer thickness and $i^2 = -1$. The total field is related to the field in the surrounding media by multiplying the $l_{m/m+1}$ and the P_m matrices. In the case of an N -layer stack surrounded by two semi-infinite media 0 and $N + 1$, the boundary conditions ($E_{N+1,-} = 0$ and $E_{\text{incident}} = E_{0,+}$) allow the calculation of the field in each layer, as a function of E_{incident} .

The Poynting's vector Σ correlates the total electromagnetic field with the electromagnetic energy transport through the stack. It's flux through an unit area of interface surface is the power flux passing through the surface. Σ is given by :

$$\Sigma = \frac{1}{2} \text{Re} \left(\mathbf{E} \times \mathbf{H}^* \right) \quad (58)$$

From Maxwell-Faraday's equation. :

$$\mathbf{H} = \frac{1}{\omega\mu} \mathbf{k} \times \mathbf{E}. \quad (59)$$

Therefore,

$$\Sigma = \frac{1}{2\omega\mu} \text{Re} \left[\mathbf{E} \times (\mathbf{k} \times \mathbf{E})^* \right]. \quad (60)$$

Here, \mathbf{E} and \mathbf{H} are the complex electric and magnetic fields, respectively, Re (Im) refers to the real (imaginary) part of such a complex vector, and '*' to the conjugation operator. At the interface between the two media, the electric field amplitude propagating in both directions E_+ and E_- , is known from the calculations given above. Hence, the flux Σ_z of Σ through any xy section can be calculated. For the transverse electric (TE) mode :

$$\Sigma_z = (1/2\omega\mu) \left[\text{Re}(k_z) \left(|E_+|^2 - |E_-|^2 \right) + 2 \text{Im}(k_z) \text{Im}(E_+^* E_-) \right], \quad (61)$$

where the permeability μ equals the permeability μ_0 of the vacuum for a non-magnetic media and k_z is the z -component of the wave-vector. For the transverse magnetic (TM) mode we have :

$$\Sigma_z = (1/2\omega) \times \left[\text{Re}(k_z/\varepsilon) \left(|H_+|^2 - |H_-|^2 \right) + 2 \text{Im}(k_z/\varepsilon) \text{Im}(H_+^* H_-) \right], \quad (62)$$

where ε is the dielectric permittivity of the medium.

The absorbance in each layer A_m of the solar cell is obtained by taking the difference of the power flux through the top and bottom interface of the layer :

$$A_m = \frac{\Sigma_{z\text{top}} - \Sigma_{z\text{bottom}}}{\Sigma_{z\text{incident}}}, \quad (63)$$

This classical thin-film method takes into account light coherence and applies to flat interface. When using this method for a-Si:H *PIN* solar cells, interference peaks are predicted in the I -layer absorbance and reflectance ($R(\lambda)$) curves. These predicted interference peaks are clearly observed in the experimental quantum efficiency $\text{QE}(\lambda)$ and $R(\lambda)$ curves of *PIN* cells deposited on smooth or moderately rough TCO.

Reflection and refraction at a rough interface : Treatment of specular and diffused components :

At a rough interface, the incident light is divided into two specular and two diffused components (Figure 5). The transverse electric (magnetic) specularly reflected and transmitted fields' amplitude coefficients r'_{TE} and t'_{TE} (r'_{TM} and t'_{TM}) are assumed to be proportional to the respective Fresnel's coefficients (eqs. (52) and (53)) with a constant of proportionality γ_{TE} (γ_{TM})

$$r'_{TE} = \gamma_{TE} r_{TE} \quad (r'_{TM} = \gamma_{TM} r_{TM}), \quad (64a)$$

$$t'_{TE} = \gamma_{TE} t_{TE} \quad (t'_{TM} = \gamma_{TM} t_{TM}). \quad (64b)$$

The factor γ_{TE} (γ_{TM}) depends on the diffused reflectance R_d and diffused transmittance, T_d at the interface, is derived by equalizing the power flux, before and after the interface. R_d and T_d are calculated from angular-resolved photometric measurements and used as input parameters to the numerical program. It is then r'_{TE} and t'_{TE} (r'_{TM} and t'_{TM}), which are to be used in eq. (56) to determine the interface matrix, $I_{m/m+1}$, when the interface is rough. Thereafter, the incident light's specular propagation is determined by the matrix formalism of Abeles [91] as already stated. The specularly reflected and transmitted light's coherence has been kept; and hence specular interferential effects (when the TCO is flat or even moderately rough) may be obtained from calculations based on this model as already stated.

In order to analyze the diffused flux, each half-space surrounding the interface is sampled in several directions (typically 40) corresponding to an incrementation of the in-plane component k_{xy} of the wave vector \mathbf{k} . k_{xy} is given

by :

$$k_{xy} = \frac{2\pi n \sin \theta}{\lambda}. \quad (65)$$

The angular diffused reflectance (transmittance) $R_d(\theta)(T_d(\theta))$ is defined as the reflected (transmitted) power around the direction θ per unit solid angle and is related to the experimentally measured quantity $R_d(T_d)$. The diffused reflected flux in the direction θ , corresponding to k_{xy} is given by

$$2\pi R_d(\theta) \sin(\theta) d\theta \Sigma_{zr,+}^0, \quad (66)$$

where $\Sigma_{zr,+}^0$ is the Poynting's vector in the positive z direction corresponding to the specular field which is known. A similar expression can be derived with $T_d(\theta)$.

The angular variation of $R_d(\theta)$ at the TCO/p interface is assumed to be Lambertian, *i.e.* it obeys the $\cos^2\theta$ law, while that for $T_d(\theta)$ is assumed to obey a $\cos^3\theta$ law. A Lambertian angular distribution law has also been assumed for both $R_d(\theta)$ and $T_d(\theta)$ at the N /aluminium or the N /silver interface. The spectroscopic distribution of these quantities, based on experimental measurements, are taken from Leblanc [52].

In the model, with the support of experimental results, it is assumed [52], that phase coherence between diffused light and incident light is lost at the rough interface. Hence this diffused light (eq. (66)) and a similar expression with $T_d(\theta)$ is similar to a 'new source' emitting within the stack. The power flux due to this 'new source' is again calculated at the top interface and the bottom interface of each layer. Thus in each layer the absorption coming from this diffusion and calculated along the k_{xy} direction is derived, as are also the new incident fluxes at rough interfaces. This procedure is continued *via* an elegant matrix method [54,52], to compute the n times diffused flux and the absorption in each layer every time. The total absorbance is finally calculated by successively adding the contribution of each step. This is the value for the generation term G in the continuity eqs. (4) and (5).

When used in conjunction with the electrical model, this method is used to calculate the energy absorbed in each of the (typically) 600 segments into which the solar cell is divided, besides the part of the incident light lost by absorption in the TCO, the back contact metal; and the reflection loss from the device. It is necessary to divide the cells into such a large number of segments to take proper account of the non-uniformity of the light absorbed in different layers, as well as the extremely

non-uniform nature of the field inside an amorphous device, resulting from carrier trapping in the large number of gap states, specially under illumination.

5.5. Solution technique :

5.5.1. Thermodynamic equilibrium :

In thermodynamic equilibrium, as already mentioned in Section 5.1, there is only the Poisson's equation (eq. (3)) to be solved. This is a second order non-linear differential equation with one dependent variable (ψ) and one independent variable (x). This equation must be solved subject to the boundary conditions (eqs. (8a) and (8b)) (mentioned in Section 5.1)

We get $\psi = \psi(x)$ by turning Poisson's equation into a set of second-order finite difference equations and using the Scarfetter and Gummel [4] method in conjunction with the Newton-Raphson technique for solving the simultaneous, non-linear equations. These latter techniques are described towards the end of this section. Once ψ is obtained, the band diagram, electric field, trapped and free carrier populations can be calculated.

5.5.2. Non-thermodynamic equilibrium steady state :

Here, the electron potential energy of the vacuum level, ψ and the quasi Fermi levels E_{Fn} and E_{Fp} are used as the dependent variables with one independent variable (x) in which the set of semiconductor equations : the Poisson's equation (eq. (3)) and the hole and electron continuity equations (eqs. (4), (5)) are to be solved. The terms in these governing equations are non-linear. The current density derivative term in the continuity equations and the vacuum level derivative term in the Poisson's equations are represented by finite central differences that couple every position in the device to the adjacent position. The three equations (eqs. (3), (4) and (5)) are coupled non-linear equations, which are to be solved using the six boundary conditions (eqs. (8c), (8d), (9a), (9b), (10a) and (10b)). The eqs. (4) and (5) contain the current densities which are given by the current density equations (eqs. (40) and (41)), the recombination term R , given by eq. (39) and the generation term G , calculated on the basis of one or the other of the optical models described in Section 5.4. However, with the expressions (40) and (41) for the current densities, numerical methods show difficulty in convergence. Scharfetter and Gummel [4] have derived a trial function for the current densities that is more convenient for obtaining numerical solutions. This method basically splits the device into two

interpenetrating lattices. On one set of grid points, we solve for the unknowns ψ , E_{F_n} and E_{F_p} , while the current densities (containing the derivatives of the quasi-Fermi levels – eqs. (40) and (41)) are solved at the other set of grid points. It then uses a direct banded matrix solution technique to solve the linearised set of equations resulting from applying the Newton-Raphson technique to the system of non linear, coupled finite difference equations. Iterative solutions are then obtained for the three coupled differential equations using the Newton-Raphson technique.

Newton-Raphson method :

This method finds the root of a function $f(x)$ iteratively, or roots of a set of functions, if given an adequate initial guess for the roots. Here, the function $f(x)$ is expanded in Taylor's series about some initial guess x_0 :

$$f(x) = f(x_0) + (x - x_0)f'(x_0) + \frac{(x - x_0)^2}{2!}f''(x_0) + \dots \quad (67)$$

Considering only the first two terms of the above equation, this technique finds the root of $f(x)$, i.e. $f(x) = 0$. Solving for x yields ultimately,

$$x - x_0 = \partial = -\frac{f(x_0)}{f'(x_0)}. \quad (68)$$

The difference between the initial guess (x_0) and the actual root (x), ∂ , is added to the initial guess (x_0) for a better estimate to the root for the next iteration. The method requires good initial guess values for the three independent variables ψ , E_{F_n} , and E_{F_p} as input. If the initial guess is close enough to the root, this method converges extremely rapidly to the desired root. The iterative procedure is stopped when the difference ∂ is less than some predetermined error criterion, h . The one-dimensional device here is divided into NPTS slabs (typically 400 to 600 slabs for single junction structures and 1000 or greater for multi-junction or NIPIN type of devices, where there is a rapid variation of one or all the dependent variables (ψ , E_{F_n} , E_{F_p}) over small distances (x)), which lead to (NPTS+1) equidistant grid points in the device where the three sets of unknowns, ψ , E_{F_n} , E_{F_p} are calculated. Since there are 6 boundary conditions, two for each unknown, at the two ends of the device, there are (NPTS–1) points in the device where the three governing equations must be solved simultaneously. Therefore, there will be (NPTS–1) \times 3 equations along

with their partial derivatives (as required in eq. (68)) to solve for the (NPTS–1) unknowns. The three eqs. ((3)–(5)) at the i -th point with the derivative terms expressed as central differences and the right hand side set equal to zero may be written respectively as :

$$F_{1i} = \frac{\psi_{i+1} - 2\psi_i + \psi_{i-1}}{\Delta x^2} - \frac{q}{\epsilon} [p_i - n_i + p_{Ti} - n_{Ti} + N_{net}^+] = 0, \quad (69)$$

$$F_{2i} = (G_i - R_i) - \frac{1}{q}$$

$$\times \left[\frac{J_{p,i+1/2} - J_{p,i-1/2}}{\Delta x} \right] = \frac{\partial p}{\partial t} = 0 \text{ at steady state,} \quad (70)$$

$$F_{3i} = (G_i - R_i) + \frac{1}{q} \left[\frac{J_{n,i+1/2} - J_{n,i-1/2}}{\Delta x} \right] = \frac{\partial n}{\partial t} = 0 \text{ at steady state,} \quad (71)$$

where Δx is the grid spacing, assumed to be the same for both the interpenetrating lattices.

The partial derivatives of F_{1i} , F_{2i} , and F_{3i} are taken with respect to every unknown non-dimensional variable (e.g. ψ_i/kT , $E_{F_n,i}/kT$, $E_{F_p,i}/kT$, at the i -th grid point). The following specific matrix equation. is then solved for the matrix X :

$$[A] \cdot [X] = [B], \quad (72)$$

where the matrix A is the Jacobian matrix of partial derivatives of the three functions F_{1i} , F_{2i} , and F_{3i} (eqs. (69)–(71)) w.r.t. each of the above-mentioned non-dimensionalised variable corresponding to the matrix X . X is constructed as :

$$\begin{bmatrix} \uparrow \\ \delta\psi_i/kT \\ \delta E_{F_n,i}/kT \\ \delta E_{F_p,i}/kT \\ \downarrow \end{bmatrix},$$

and the matrix B constructed as :

Table 1. Parameters extracted using ASDMP to simulate the experimentally measured characteristics of a standard a-Si:H based single junction *PIN* solar cell.

Parameter	<i>P</i> -a-SiC:H	<i>I</i> -a-SiC:H (buffer)	<i>I</i> -a-Si:H (IL ^a)	<i>I</i> -a-Si :H	<i>N</i> -a-Si:H
Layer thickness (nm)	8	3	10	990	20
Electron affinity (eV)	3.89	3.88	4.00	4.00	4.00
Mobility gap (eV)	2.00	2.00	1.86	1.86	1.80
Activation energy (eV)	0.46	0.46	0.87	0.87	0.21
Effective DOS in valence and conduction bands (cm ⁻³)	2.0×10^{20}	2.0×10^{20}	2.0×10^{20}	2.0×10^{20}	2.0×10^{20}
Characteristic energy (VB tail) (eV)	0.120	0.110	0.050	0.050	0.050
Characteristic energy (CB tail) (eV)	0.070	0.055	0.030	0.030	0.030
Exponential tail prefactors G_{D0} , G_{A0} (cm ⁻³ eV ⁻¹)	4.0×10^{21}	4.0×10^{21}	4.0×10^{21}	4.0×10^{21}	4.0×10^{21}
Electron mobility (cm ² /V s)	20	20	30	30	30
Hole mobility (cm ² /V s)	2	4	5	5	5
DOS (cm ⁻³) (annealed state)	8×10^{18}	5×10^{17}	2×10^{17}	5×10^{15}	9×10^{18}
DOS (cm ⁻³) (stabilized state)	8×10^{18}	5×10^{17}	2×10^{17}	1×10^{17}	9×10^{18}
Neutral σ^b (tails) (cm ²)	10^{-15}	10^{-15}	10^{-17}	10^{-17}	10^{-17}
Charged σ^b (tails) (cm ²)	2×10^{-15}	2×10^{-15}	10^{-16}	5×10^{-17}	10^{-16}
Neutral σ^b (midgap) (cm ²)	10^{-15}	10^{-15}	5×10^{-16}	10^{-16}	10^{-17}
Charged σ^b (midgap) (cm ²) (annealed)	2×10^{-15}	2×10^{-15}	5×10^{-14}	5×10^{-15}	10^{-16}
Charged σ^b (midgap) (cm ²) (stabilized)	2×10^{-15}	2×10^{-15}	5×10^{-14}	10^{-14}	10^{-16}

^aIL stands for 'intermediate layer', defined in the text.

^b σ is the capture cross section of a given defect state.

Table 2. Calculated values of the dark current density from the 1.0 μm *PIN* cell at a reverse applied voltage of 2 volts and a forward applied voltage of 1 volt, for different values of the dangling bond (DB) density in the intrinsic absorber.

Applied voltage (volts)	Dark current (mA cm ⁻²)			
	Low DB density		High DB density	
	HFE*	no HFE*	HFE*	no HFE*
-2.0	9.83×10^{-9}	2.29×10^{-9}	3.17×10^{-7}	5.07×10^{-8}
1.0	1.78		0.44	

*HFE stands for high field enhancement at reverse bias.

$$- \begin{bmatrix} \uparrow \\ F_{1,i} \\ F_{2,i} \\ F_{3,i} \\ \downarrow \end{bmatrix}.$$

The matrices are set up in this manner so that the Jacobian matrix A is a banded matrix. This minimizes the amount of computer time necessary to invert the matrix A to solve for the matrix X . After each iteration, the matrix X is added to the latest guess until the smallest value contained within the matrix X is less than some predetermined error criterion h . Here, h is taken to

be equal to 10^{-6} in the non-thermodynamic equilibrium steady state and 10^{-9} in thermodynamic equilibrium for all the non-dimensionalized unknowns.

6. Typical results for a single junction a-Si:H based solar cell : calculations based on ASDMP

Typical results obtained for a standard single junction a-Si:H based *PIN* structure solar cell using the above model are described in this section. The cell chosen is an $\sim 1.0 \mu\text{m}$ standard *PIN* cell of structure : *P*-a-SiC:H/*I*-a-SiC:H(buffer)/*I*-a-Si:/*N*-a-Si:H. In addition, the first 10 nm of the intrinsic layer is assumed to have a dangling bond density intermediate between the DOS in the buffer and that in the main *I*-layer. This layer will be referred to as the 'intermediate layer' (IL).

The input parameters as extracted by modeling the measured dark and illuminated current density-voltage (J - V) as well as the quantum efficiency (QE) characteristics of this cell in the annealed and light-stabilized states are given in Tables 1 and 2. The front and back contact barrier heights are taken to be 1.34 eV and 0.21 eV, respectively.

The calculated values of the dark current at a reverse bias of 2 volts, both with and without the high field

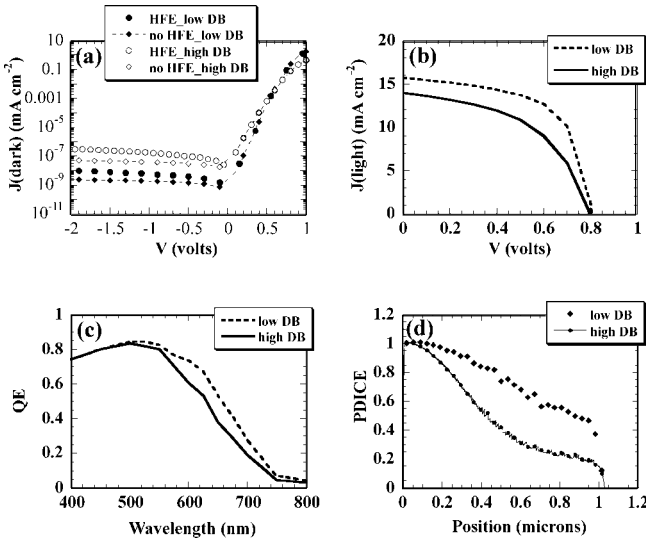


Figure 6. Different characteristics of the $1 \mu\text{m}$ PIN cell having a standard a-Si:H *I*-layer in the annealed state (*i.e.*, when the dangling bond (DB) DOS is low) and in the light-stabilized state (high DB density with increased charged capture cross section): (a) the dark J - V characteristics – the current at reverse bias has been calculated both by taking into account high field enhancement (HFE) *via* the Poole-Frenkel effect, and when this effect is absent (no HFE), (b) the light J - V characteristics, (c) the QE characteristics at 0 volts and (d) the PDICE at 0 volts. All quantities in (b), (c) and (d) have been calculated under AM 1.5 light.

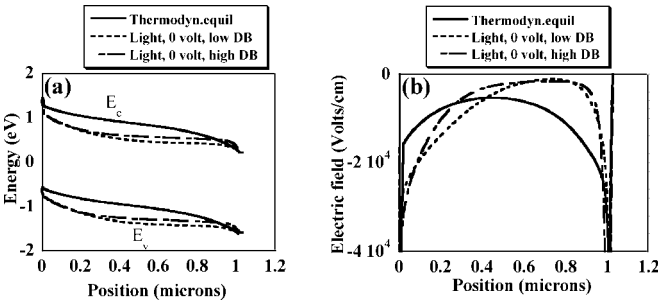


Figure 7. (a) The band diagrams of the $1 \mu\text{m}$ PIN cell having a standard a-Si:H *I*-layer in the annealed state (*i.e.*, when the dangling bond (DB) DOS is low) under thermodynamic equilibrium and under AM1.5 illumination at 0 volts and of the same cell after prolonged light-soaking (high DB density with increased charged capture cross section) under AM 1.5 light, 0 volts and (b) the electric field within the device under the same three conditions.

enhancement (HFE) effect, taken into account *via* the Poole-Frenkel mechanism in the model ASDMP, are given in Table 2 in the annealed (low dangling bond (DB) density) and light-stabilized (high DB density) states. Dark current densities at a forward bias of 1 volt are also given under these two conditions.

Figure 6(a) gives the dark J - V characteristics of the $1.0 \mu\text{m}$ PIN cell considered, as calculated on the basis of model ASDMP, in the annealed and light-stabilized states. The calculated light J - V characteristics

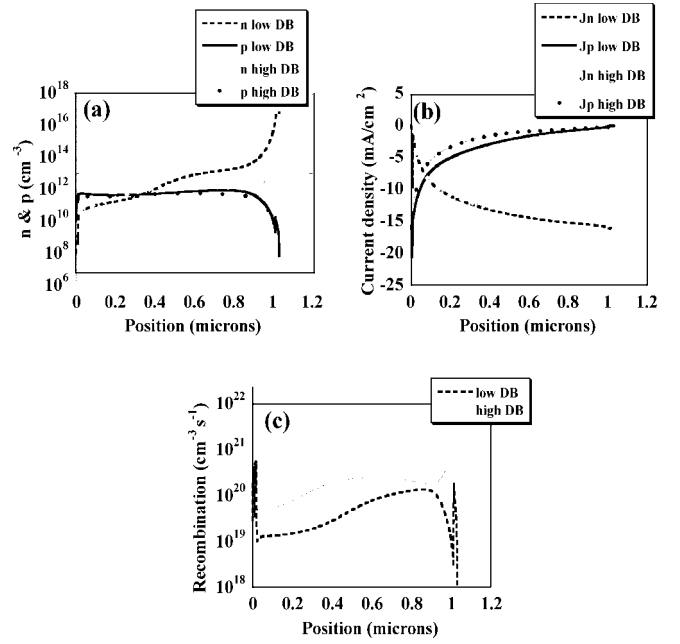


Figure 8. (a) The free electron and the hole densities, (b) the electron and hole current densities and (c) the recombination in the device in the annealed (low DB) and light-stabilized (high DB) states under illumination and 0 voltage bias.

(Fig. 6(b)) of the cell yield a short-circuit current density of $J_{sc} = 15.73 \text{ mA/cm}^2$, open-circuit voltage $V_{oc} = 0.806$ volts, fill-factor $FF = 0.601$, and efficiency $\eta = 7.629\%$ in the annealed state. In the same graph, the light J - V characteristic in the degraded condition of the cell is also shown. Except for the open-circuit voltage, all the other solar cell output parameters are found to deteriorate considerably. The model yields the following values under this condition: $J_{sc} = 13.97 \text{ mA/cm}^2$, $V_{oc} = 0.798$ volts, $FF = 0.487$, $\eta = 5.44\%$. Figure 6(c) shows the quantum efficiency (QE) under AM1.5 illumination at 0 volts, in the annealed and light-soaked states of the given cell, as calculated on the basis of our model. As expected, the QE after prolonged light-soaking deteriorates over the middle and long wavelength regions of the solar spectrum, due to increased recombination in the intrinsic layer on account of the increase of the mid-gap defect density and the charged capture cross section of these states in the intrinsic layer (Table 1). The short wavelength QE (SWQE) however, remains unaffected. This is because light of this wavelength is mainly absorbed in the first 100 nm of the device and in part of this region (P -layer, buffer, IL), the DOS and σ are unchanged (Table 1). Over that part of the I -layer, immediately adjoining the IL , the dangling bond (DB) DOS of course does increase; however the higher DOS also leads to increased hole trapping and hence a higher electric field over a narrow

front region (Figure 7(b)), than that which existed here in the annealed state. This stronger field annuls to some extent the negative effect of the increased DB density over the first ~ 100 nm; hence the SWQE in the light-soaked state does not fall relative to that in the annealed state (Figure 6(c)). Figure 6(d) shows the position-dependent inner collection efficiency in the annealed and light-soaked states. Carrier collection is seen to deteriorate in the middle and back of the device (Figure 6(d)) with an increase of the dangling bond density and their charged capture cross-section, in the light-stabilized state.

However PDICE in the front remains unaltered due to the same reason as mentioned above for the case of the SWQE.

The band diagrams at thermodynamic equilibrium in the annealed condition, and at the steady state under illumination both in the annealed (low DB) and light-soaked (high DB) states, are compared in Figure 7(a). We find that the bands under illumination become flatter than those obtained under thermodynamic equilibrium. When the dangling bond density is high, as *e.g.* after light-soaking, the bands become flatter still. This is because, under illumination, due to excess hole trapping near the P/I interface a stronger field develops over this region, relative to that at thermodynamic equilibrium (Figure 7(b)); and this in turn leads to a collapse of the bulk electric field. The dangling bond density increases on light-soaking (high DB case in the Figure), leading to further hole-trapping at the P/I interface and a progressively lower field in the bulk. This is seen in Figure 7(b), where the electric field within the device is plotted at thermodynamic equilibrium and under illumination in the annealed and light-soaked states. The free electron and hole density (n and p) profiles, the electron and hole current densities and recombination in the device for the two cases (annealed and light-soaked) are shown in Figures 8(a-c) respectively under illumination and 0 voltage bias.

7. Summary

In this review, we have shown how detailed computer modeling can be used to simulate the output characteristics of semiconductor devices, such as the dark and illuminated current density-voltage and quantum efficiency curves under different light and voltage bias conditions. The parameters extracted by simulating the experimental characteristics can then be utilized to gain an insight into the working of the device, understand the factors which

may be responsible for the possible under-performance of a device, and in general, suggest ways of optimizing the device performance. These extracted parameters can also be used to calculate the electric field, the recombination, the free and trapped charge densities, and the electron and hole current densities as a function of position inside the device-quantities that cannot be determined experimentally. Such insight and suggestions from modeling calculations help experimentalists improve device performance, with a minimum of trial runs. We have in this review, described one such typical model – ‘Amorphous Semiconductor Device Modeling Program (ASDMP)’ – capable of simulating both the electrical and optical properties of semiconducting opto-electronic devices.

8. Future outlook

The future of computer modeling of semiconductor devices lies in predicting novel designs and new combinations for improved device performance. A case in point is the concept of band gap profiling introduced by Guha’s group [92], which brought into focus the hugely successful and relatively high efficiency amorphous silicon/amorphous silicon-germanium tandem solar cells. As semiconductor design becomes more and more complicated, it becomes extremely time-consuming and expensive to optimize device design. As already stated, such efforts on the part of experimentalists can be vastly reduced with the help of detailed computer modeling. We may cite the example of the amorphous silicon/crystalline silicon heterojunction with Intrinsic Thin layer (HIT) cells, discovered by the Japanese group – Sawada *et al* [93]. These cells combine the high efficiency of crystalline silicon solar cells and the low cost of amorphous silicon cells. In fact conversion efficiencies as high as 20.7% have been achieved by the Sanyo group [94]. In such cells there are several interfaces and the design is extremely complex, so that detailed electrical and optical modeling, using a model such as ASDMP described here, is indispensable for their optimization.

Acknowledgments

The authors acknowledge valuable discussions with Dr. P Roca i Cabarrocas of the Ecole Polytechnique, Palaiseau, France and Profs. A K Barua and Swati Ray of the Indian Association for the Cultivation of Science, Kolkata, India. The computer modeling program was developed by P Chatterjee during the course of a project funded by the Ministry of Non-Conventional Energy Sources and the Department of Science and Technology, Government

of India.

References

- [1] M Kurata *Numerical Analysis for Semiconductor Devices* (Lexington, MA : Lexington Books) (1982)
- [2] S Selberherr *Analysis and Simulation of Semiconductor Devices* (New York : Springer-Verlag) (1984)
- [3] G A Swartz *J. Appl. Phys.* **53** 712 (1982)
- [4] D L Scharfetter and H K Gummel *IEEE Transactions on Electronic Devices* **ED16** 64 (1969)
- [5] W Shockley and W T Read *Phys. Rev.* **87** 835 (1952)
- [6] R N Hall *Phys. Rev.* **87** 367 (1952)
- [7] I Chen and S Lee *J. Appl. Phys.* **53** 1045 (1982)
- [8] R S Crandall *J. Appl. Phys.* **54** 7176 (1983)
- [9] H Okamoto, H Kida, S Nonomura and Y Hamakawa *Solar Cells* **8** 317 (1983)
- [10] P Sihanugrist, M Konagai and K Takahashi *J. Appl. Phys.* **55** 1155 (1984)
- [11] P Sihanugrist, M Konagai and K Takahashi *Sol. Energy Mater.* **11** 35 (1984)
- [12] B W Faughnan and R S Crandall *Appl. Phys. Lett.* **44** 537 (1984)
- [13] B Faughnan, A Moore and R S Crandall *Appl. Phys. Lett.* **44** 613 (1984)
- [14] T Ikegaki, H Itoh, S Muramatsu, S Matsubara, N Nakamura, T Shimada, J Umeda and M Migitaka *J. Appl. Phys.* **58** 2352 (1985)
- [15] M Hack and M Shur *J. Appl. Phys.* **58** 997 (1985)
- [16] G W Taylor and J G Simmons *J. Non-Cryst. Solids* **8-10** 940 (1972)
- [17] R J Schwartz, J L Gray, G B Turner, D Kanani and H Ullal *Proceedings of the 17th IEEE Photovoltaic Specialists Conference (Kissimmee) 1st-4th May* p 369 (1984)
- [18] C T Sah *Proc. of the IEEE Electron Devices* **55** 672 (1967)
- [19] A H Pawlikiewicz and S Guha *Proc. of the 20th IEEE Photovoltaic Specialists Conference (Las Vegas, NV) 26th-30th September* p251 (1988)
- [20] H Tasaki, W Y Kim, M Hallerdt, M Konagai and Y Yamamoto *J. Appl. Phys.* **63** 550 (1988)
- [21] K Misiakos and F A Lindholm *J. Appl. Phys.* **64** 383 (1988)
- [22] P J McElheny, J K Arch, H -S Lin and S J Fonash *J. Appl. Phys.* **64** 1254 (1988)
- [23] P J McElheny, P Chatterjee and S J Fonash *J. Appl. Phys.* **69** 7674 (1991)
- [24] P Chatterjee, P J McElheny and S J Fonash *J. Appl. Phys.* **67** 3803 (1990)
- [25] J Y Hou, J K Arch, S J Fonash, S Wiedeman and M Bennet *Proc. of the 22nd IEEE Photovoltaic Specialists Conference (Las Vegas, NV) 7th-11th October* p1260 (1991)
- [26] F A Rubinelli, S J Fonash and J K Arch *6th Intl. Photovoltaic Science and Engineering Confermce* (New Delhi, India) 10th - 14th February p 811 (1992)
- [27] J K Arch, F A Rubinelli, J -Y Hou and S J Fonash *J. Appl. Phys.* **69** 7057 (1991)
- [28] A Mittiga, P Fiorini, M Falconieri and F Evangelisti *J. Appl. Phys.* **66** 2667 (1989)
- [29] H Kida, M Itoh, S Fukazawa, T Ohta and K Yamamoto *Jpn. J. Appl. Phys.* **28** L 1499 (1989)
- [30] P Chatterjee *6th Intl. Photovoltaic Science and Engineering Confermce* (New Delhi, India) 10th -14th February p329 (1992)
- [31] P Chatterjee *J. Appl. Phys.* **75** 1093 (1994)
- [32] P Chatterjee *J. Appl. Phys.* **79** 7339 (1996)
- [33] N Palit and P Chatterjee *J. Appl. Phys.* **86** 6879 (1999)
- [34] P Chatterjee, R Vanderhagen and B Equer *Mat. Res. Soc. Symp. Proc.* **420** 233 (1996)
- [35] P Chatterjee, R Vanderhagen and B Equer *J. Appl. Phys.* **87** 1874 (2000)
- [36] F Smole and J Furlan *J. Appl. Phys.* **72** 5964 (1992)
- [37] F Smole and J Furlan *Sol. Energy Mater. Sol. Cells.* **34** 385 (1994)
- [38] M B von der Linden, R E I Schropp, Van W G J H M Sark, M Zeman, G Tao and J W Metselaar *Proc. of the 11th European PVSEC (Montreux)* p647 (1991)
- [39] M Zeman, J A Willemen, S Solntsev and J W Metselaar *Tech. Digest of the 7th Intl. PVSEC* p609 (1993)
- [40] M Zeman, J A Willemen, S Solntsev and J W Metselaar *Sol. Energy Mater. Sol. Cells* **34** 557 (1994)
- [41] J A Willemen, M Zeman and J W Metselaar *Proc. of the 1st World Conference on Photovoltaic Solar Energy Conversion, Proc. of the 24th IEEE Photovoltaic Specialists Conference (Waikoloa, HI, USA) 5th-9th December* p599 (1994)
- [42] G A M Hurkx, D B M Klaassen and M P G Knuvers *IEEE Transactions of Electron Devices* **39** 331 (1992)
- [43] H Antoniadis, R I Devlen, S Esipov, S Guha, E A Schiff and J Tauc *ICAS-14*, (1991)
- [44] G Juška, J Kocka, K Arlauskas and G Jukonis *Sol. State. Commun.* **75** (1990)
- [45] R Martins, A Fantoni and M Vieira *J. Non-Cryst. Solids* **164-166** 671 (1993)
- [46] A Kreisel *Master's Thesis* (Forschungszentrum, Jülich, Institut für Schicht und Ionentechnik) May (1995)
- [47] O S Heavens *Optical Properties of Thin Solid Films* (London : Butterworths) (1955)
- [48] E Yablonovitch *J. Opt. Soc. Am.* **72** 899 (1982)
- [49] E Yablonovitch and G D Cody *IEEE Trans. Electron. Devices* **29** 300 (1982)
- [50] H W Deckman, C R Wronski, H Witzke and E Yablonovitch *Appl. Phys. Lett.* **42** 968 (1983)
- [51] H Shade and Z Smith *J. Appl. Phys.* **57** 568 (1985)
- [52] F Leblanc *These de Docteur en Science, Université de Paris-Sud Centre, d'Orsay* (1992)
- [53] F Leblanc, J Perrin, E Cornil and J Schmitt *MRS Spring Meeting* (San Francisco, USA) April (1992)
- [54] F Leblanc, J Perrin and J Schmitt *J. Appl. Phys.* **75** 1074 (1994)
- [55] F A Rubinelli, J Daey Ouwens and R E I Schropp *13th European Photovoltaic Solar Energy Conference* (Nice, France) October 23th-27th p195 (1995)
- [56] P Chatterjee, F Leblanc, M Favre and J Perrin *Mat. Res. Soc. Symp. Proc.* **426** p593 (1996)
- [57] G Tao, M Zeman, and J W Metselaar *Sol. Energy Mater. Sol. Cells* **34** 359 (1994)
- [58] H Stiebig, A Kreisel, K Winz, N Schultz, C Beneking, T Eickhoff and H Wagner *Proc. of the 1st World Conference on Photovoltaic Solar Energy Conversion, Proc. of the 24th IEEE Photovoltaic Specialists Conference (Waikoloa, HI, USA) 5th -9th December* p603 (1994)

About the Reviewers

Dr. N. Palit, a former IIT-ian and researcher under Prof. Parsathi Chatterjee, obtained her PhD in Physics from the Jadavpur University on computer modeling of solar cells. She has published around 12 papers in different international and national journals and conferences. At present she is a lecturer in Contai P K College, Midnapur.

Ms. Ushasi Dutta has been a research scholar under Prof. Parsathi Chatterjee of the Energy Research Unit, Indian Association for the Cultivation of Science, Kolkata, India, since 2001 and has obtained the PhD degree of Jadavpur University, India in November, 2005. She has published 5 papers in different international journals and has 3 international conference papers. Her present interest of research is computer modeling of single and multi-junction solar cells.

Prof. Parsathi Chatterjee is the present Head of the Energy Research Unit, Indian Association for the Cultivation of Science, Kolkata. Her present field of interest is computer modeling of semiconductor devices based on disordered semiconductors and the new group of amorphous silicon/crystalline silicon 'Heterojunction with Intrinsic Thin Layers (HIT)' solar cells. She obtained her PhD degree in 1977, doing theoretical research on electronic energy states in solids. Her significant contribution in this field is the extension of the Gilat-Raubenheimer method of calculating the density of states to metals with the hexagonal-close-packed structure. She then switched over to experiments on ion implantation to produce metallic glasses and to high T_c superconductors in thin film form. She has more than 57 papers in reputed international journals and in the proceedings of international conferences. She is a recipient of the National Science Talent Search fellowship of the Government of India and Marie Curie fellowship of the European Community.